

Experimental and Theoretical Investigation of Mechanism of Kinesin Motility.

Anna Kinga Labno

Submitted to the Department of Physics in partial fulfillment of the requirement for the degree of


Bachelor of Science

at the
Massachusetts Institute of Technology
Cambridge, May 2007

[June 2007]

©2007 Anna Labno
All rights reserved

The author hereby grants to MIT permission to reproduce and to distribute publicly paper and electronic copies of this thesis document in whole or in part in any medium now known or hereafter created.

Signature of Author 

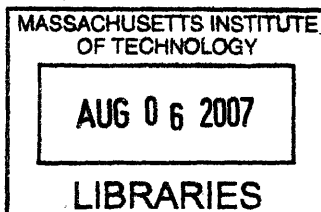
Anna K. Labno
Departments of Physics and Biology
May 18, 2007

Certified by 

Professor Matthew J. Lang
Thesis Supervisor
Departments of Biological and Mechanical Engineering

Accepted by

Professor David E. Pritchard
Senior Thesis Coordinator
Department of Physics



ARCHIVES

"Tak moja postać, im dalej ucieka

Tym grubszym kirem twa pamięć pomroczy" (Adam Mickiewicz)

To the loved ones far away.

Contents

1	Introduction	1
1.1	Kinesin Structure	2
1.2	Early Studies of Kinesin	5
1.3	Single Molecule Kinesin Studies	6
1.3.1	Conventional Kinesin Walks using Asymmetric Hand-over-hand mechanism	6
1.3.2	Mutations in Neck Linker result in impaired motility of Kinesin while the ATPase and MT binding remains undisturbed.	8
1.3.3	Neck Linker Plays Crucial Role in Motility	9
1.3.4	Changes in switch I and II due to ATP binding lead to zipper-like docking of NL	10
1.4	Optical Trapping Technique	10
2	Proposed Mechanism of Kinesin Motility	12
2.1	Structural Analysis	12
2.2	Molecular Dynamics Simulation	13
2.3	Proposed Mechanism for Kinesin Motility	15
3	Experimental Design	16
3.1	Protein Engineering	16
3.1.1	Mutant Design	16
3.1.2	Cloning	18
3.1.3	Protein Expression and Purification	18
3.1.4	Microtubule Preparation	19
3.1.5	Bead Assay	20
3.2	Optical Trapping	20
3.2.1	Trap Design	22
3.2.2	Position Calibration	22

<i>CONTENTS</i>	2
3.2.3 Stiffness Calibration	24
3.2.4 Trapping Assays	24
4 Unloaded Velocity Measurements	25
4.1 Data Acquisition and Analysis	25
4.2 Results	27
5 Loaded Velocity Measurements	28
5.1 Data Acquisition and Analysis	28
5.2 Results	30
6 Stall Force Measurements	33
6.1 Data Acquisition and Analysis	33
6.2 Results	33
7 Processivity	35
7.1 Data Acquisition and Analysis	35
7.2 Results	35
8 Stepping Characteristics	37
8.1 Data Acquisition and Analysis	37
8.2 Results	37
9 Conclusions and Future Work	40

Acknowledgments

The author would like to thank Prof. Lang for his excellent guidance throughout this research project. I am also very grateful to Ahmed Khalil and Dave Appleyard for conducting experiments with me, sharing their expertise and providing useful advice. Guichy Waller contributed much through helpful discussion about protein purification and Wonmunk Hwang was instrumental in mutant design. Special thanks also go to Jakub Kominiarczuk for helpful discussion regarding data analysis. I would like also to express my thanks to members of Lang lab Carlos Castro, Ricardo Brau, Jorge Ferrer, Peter Tarsa and Ding Fangyuan who were always very helpful and generous with their time. I am very appreciative of help and support of Prof. Belcher and Prof. Matsudaira who kindly allow me to conduct portions of the experimental work in their laboratory.

Abstract

Kinesin is a motor protein capable of utilizing chemical energy from ATP hydrolysis to generate mechanical force to power its progressive motility along a microtubule track. The mechanism of motility has been a subject of extensive study for last decade. Recently, it has been proposed that novel element—cover strand—is essential in power-stroke-like force generation. In this work we attempt an experimental verification of this hypothesis by studying the mechanical properties, such as unloaded velocity, force velocity relationship, stall forces, processivity and step size of kinesin and mutants targeting cover strand region. We show that A9G and D11G mutants move slower and have lower stall force than the wild type molecule, but the mutants are ultraprocessive, make steps of 7nm and have a higher probability of taking backward steps suggesting that, indeed, force generating mechanism might be adversely affected by this mutation but it could also affect flexibility and directionality of the molecule.

Chapter 1

Introduction

Motor proteins are enzymes that are responsible for molecular transport. Those proteins convert the chemical energy derived from the hydrolysis of ATP directly into mechanical work and are necessary for the eukaryotic cell to achieve complex organizational and structural tasks. Motor proteins allow efficient transport of molecular structures and organelles such as vesicles, mitochondria, and chromosomes which is necessary since diffusion is too slow to efficiently move material from one part of the cell to another on a physiological time scale [1]. This ability to control cellular transport processes and cell structure allowed for the development of complex cellular organelles like cilia or flagella in single-cell organisms and made possible the development of multi-cellular organisms with highly specialized cells. Those molecular motors have served as an important model system for understanding biological motility.

Microtubule-based motors of the kinesin superfamily are involved in intracellular transport, mitosis and meiosis, control of microtubule dynamics and signal transduction pathways [2]. Kinesin transports a variety of cargo such as lysosomes, melanosomes, synaptic vesicle precursors, chromosomes as well as mRNA, intermediate filaments, and signaling molecules [2]. Kinesins are also involved in chromosome and cytoskeleton rearrangements and play a role in vesicle transport in the secretory pathway [4]. Mutations in neuronal kinesin have been implicated in various neurological diseases [3]. Because of their biological importance and interesting chemistry, kinesins are the subject of extensive research, including studies aimed at understanding the molecular mechanisms of motility and their coordination and regulation.

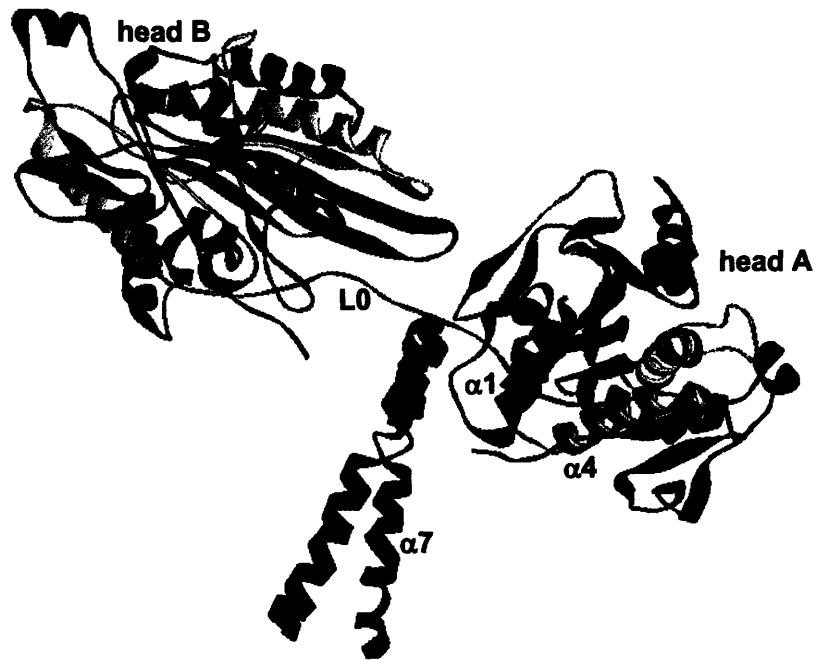


Figure 1.1: Crystal structure of the rat kinesin dimer (KIN3). The motor heads A and B are connected to the coiled coil $\alpha 7$. The $\alpha 4$ residue is of the motor head is marked in green. The coiled-coil pointing to the left side has a twofold symmetry. However, the heads are related by a rotation of nearly 120 degree. The rat kinesin and *Drosophila ncd* studied in this work have very similar motor domain core structures but differ slightly in linker regions.

1.1 Kinesin Structure

In its native form, conventional kinesin is a homodimer (120 kDa) consisting of two identical heavy and light chains. Kinesin's heavy chain contains seven functional domains. The motor domain (head domain) spans amino acids 1-344 and includes the ATP and the microtubule binding sites and is sufficient for motility and it is homologous in all known kinesins [5] and bears structural similarity to the nucleotide-binding core of the actin-based motor myosin, suggesting that these two motors could share a common ancestor [6, 7]. The presence of signature sequence in the domain core is basis for classification of proteins into kinesin superfamily. The second domain is the

dimerization domain (stalk) which is encoded by amino acids 345-380 and forms parallel coiled dimer. This α -helical coiled coil is interrupted by non-helical regions that are responsible for dimerization of the two subunits [77]. Following that there is the neck linker domain which has been suggested to be important for kinesin force generation by undergoing conformational changes upon nucleotide binding and unbinding that enable motor stepping [30]. This region is also implicated to play a role in motion directionality [8, 9, 10]. The neck linker is in turn connected to another domain; a coiled coil structure in which coil 1 (aa 437-556) and coil 2 (600-910) were long suspected to form coiled-coils as they have high α -helix content as determined by circular dichroism and are likely to form elongated, parallel dimers as shown by electron microscopy studies. This coiled coil leads to the cargo-binding domain [5]. It is thought that Coil 2 binds light chains via tetrameric coil-coil [39], which then in turn bind specifically to cargo [75, 2]. The motor system is completely contained in the heavy chains and if the heavy chain gene of *Drosophila* kinesin is expressed and purified without the light chains, the resulting protein forms dimers and moves at the same speed as full protein.

Atomic resolution crystal structures were first obtained for motor domain monomers of human kinesin [28] and then *Drosophila* ncd [37]. The structures share significant homology and in both cases the motor domain has approximate dimensions of 70 Å 45 Å 45 Å (Figure 1.2) with a back laid by eight-stranded β -sheet flanked on each side by three major α -helices. Obtaining high resolution structures of kinesin dimers was more challenging but currently three are available: one from rat [30] and two of the *Drosophila* ncd dimer [30, 31]. In all three cases, dimerization is mediated by the formation of a coiled coil by the helices $\alpha 7$ as shown on figure 1.1. Kinesin core starts from strand $\beta 1$ and terminates at long helix $\alpha 6$ which corresponds to residues 107324 for rat kinesin and 349670 for ncd. When the structure of rat kinesin was uncovered [34, 30] three, previously unseen β -strands, $\beta 0$, $\beta 9$ and $\beta 10$, were found outside the motor domain core. $\beta 0$ is at the N-terminal end of the core which immediately leads into $\beta 1$, while $\beta 9$ and $\beta 10$ link major helix $\alpha 6$ at the C-terminal to the coiled coil structure $\alpha 7$. The two motor domains of the dimer are relatively close to each other as they are separated by an angle of $\approx 120^\circ$. The *Drosophila* ncd dimer displays quasi two-fold mirror symmetry [31] with respect to central plane through the axis of the coiled coil. The coiled coil is connected to the core by the short loop L0 (Arg 346 Asn 348) between $\alpha 7$ and $\beta 1$. Many residues sticking out into this region interact with the motor domain core through unstructured loops L6,

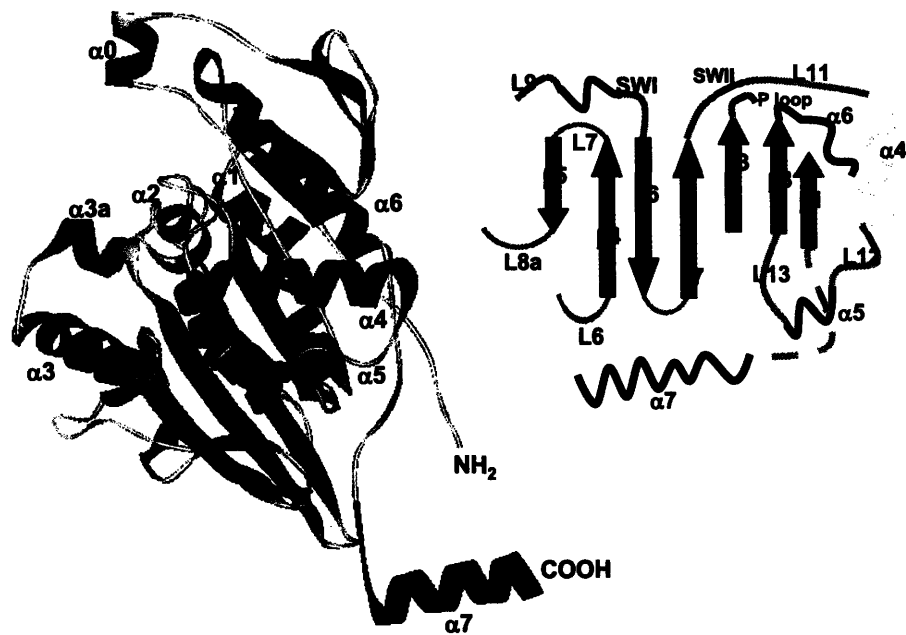


Figure 1.2: A. Crystal structure of the *Drosophila* ncd motor head. The P loop is the conserved motif that forms the nucleotide binding cleft. Neck linker consists of $\beta 9$ and $\beta 10$. In the bound conformation, β -sheets are formed between $\beta 9$ and the N-terminal $\beta 10$ and $\beta 7$ that runs along motor core. $\alpha 4$ (olive) is marked for orientation and comparison with Figure 1.1 B. Topology of the central β sheet and interconnecting secondary structural elements. The color coding of α helices corresponds to crystal structure (A).

L10, L13 and helix $\alpha 1$. In the $\beta 9\beta 10$ linker region, many residues, especially those interacting with the core and seven residues in the $\alpha 7$ helices are quite strictly conserved through kinesin superfamily.

1.2 Early Studies of Kinesin

Early research of kinesin motility aimed to elucidate mechanical principles of motor operation by investigating the structural, chemical and mechanical properties of it. It has been postulated quite early that reaction responsible for powering of kinesin must be of cyclic nature and involve binding and unbinding of the motor since kinesin can travel on microtubule a distance much larger than its dimensions [75]. Kinesin step size, which is defined as the distance between consecutive motor-binding sites on the microtubule was predicted to be 8nm based on the fact that kinesin follows the microtubule protofilament axis [40, 41] and there is only one binding site per tubulin dimer [44, 42] so the most likely step size is the distance between tubulin dimers (8nm) or a multiple of that distance. Rotation experiments showed that the steps are both co-linear and equally spaced [43] implying that both heads must make identical steps, furthermore it would be unlikely if step size drastically exceeded protein dimension 8nm step is more likely then a multiple. The force generated by kinesin stepping at various viscous loads was measured by increasing the viscosity of the solution through which a kinesin moved and so increasing the load felt by the microtubule. Slowing down of longer microtubules at high viscosity allowed to extrapolate to force at which velocity was expected to be zero (stall force) which was estimated to be 4 to 5 pN [45]. If we assume that each step is associated with the hydrolysis of one ATP molecule, the efficiency of kinesin motor is approximately 40% [75], which is comparable to other biological processes utilizing ATP [47]. Experiments with directional loading of the kinesin motor as it buckles a microtubule showed that the speed increased meaning that the perpendicular load catalyzes the forward reaction [46]. This suggest that the hydrolysis cycle is slowed down at high loads resulting in decreased stepping rate rather than decreased velocity of the step.

The role of kinesin two heads was also extensively studied in order to answer the question whether kinesin's two headed structure was indeed crucial for motility. The processivity of the kinesin showed by dilution experiments [48, 41], implies that each motor spends little time detached from the filament suggesting that two heads are vital for kinesin to remained attached to

microtubule through some, either coordinated or uncoordinated mechanism. Kinesin motor domain, with dimerization and coil domains deleted, moves around 80 % slower than the full length dimeric protein and switches randomly between adjacent protofilaments more often [49]. The isolated motor domain does not move at all in low density assays. This further reinforces the notion of interaction between the two heads. Negative cooperativity between two nucleotide binding sites was shown by demonstrating alternating head catalysis during microtubule stimulated ATP hydrolysis [15] implying that cooperative interaction between two heads is more likely.

1.3 Single Molecule Kinesin Studies

Development of single molecule techniques in subsequent years allowed for direct verification of bulk assays observations and for investigation of detailed molecular description of kinesin motor function. Results from variety of single-molecule experiments has confirmed mechanochemical properties of kinesin motors as postulated before. It has been directly demonstrated that conventional kinesin is a highly processive motor that can take more than 100 consecutive 8.2-nm steps along microtubule [11, 12] consuming exactly 1 ATP per step [54, 117]. Kinesin still moves under loads of up to 6 pN [120, 25] and it is 40-50% efficient in converting the energy of ATP hydrolysis into forward mechanical work on the microtubule.

1.3.1 Conventional Kinesin Walks using Asymmetric Hand-over-hand mechanism

The notion that in order to take many consecutive steps along the microtubule without dissociating, the two heads must operate in a coordinated manner has been substantiated by demonstrating coordination between the two motor domains in the kinesin dimer [49, 13, 14], and an alternating-site enzymatic mechanism has been proposed [55, 16, 17]. Moreover it was observed that the enzyme cannot freely slide in the direction of the microtubule axis [70] and this allows it to move processively even under substantial load which is probably a reflection of the fact that in the cell it has to often overcome viscous forces imposed by mechanical obstructions to organelle movements inside cells.

Two models for how kinesin heads are coordinated have been postulated: the hand-over-hand “walking” model in which the two heads alternate in the

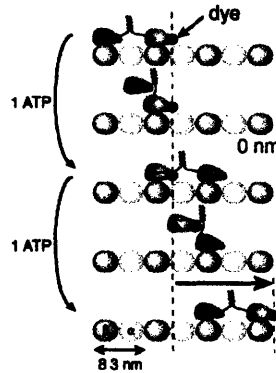


Figure 1.3: The hand over hand model for kinesin walking. This model predicts that a dye on the head of kinesin will move alternately 16.6nm, 0nm, 16.6nm etc., in contrast to inchworm mechanism in which the dye would always move 8.2nm. FRET experiments by Yildiz *et al* confirmed that kinesin, indeed moves by asymmetric hand over hand mechanism. Figure adopted from [81]

lead [77], and an inchworm model in which one head always leads [53]. The hand-over-hand model predicts that, for each ATP hydrolyzed, the rear head moves twice the center of mass, whereas the leading head does not move at all [53, 55]. To differentiate between mechanisms, stalk rotation was measured by immobilizing kinesin molecules by the distal end of the neck and examining the extent of microtubule rotation relative to the immobilized neck. The inchworm model and asymmetric hand over hand model predicts that the stalk rotation does not take place while symmetric hand-over-hand model predicts 180° around its axis for every 8-nm step. No rotation was detected indicating inconsistency with the symmetric hand-over-hand model [53]. First direct evidence of a model in which the roles of the two heads alternate every 8-nm step was provided by Kaseda and coworkers. They made a heterodimeric kinesin with an altered nucleotide-binding motif. Although the mechanochemical cycle rates of each head are significantly different the heterodimer moves processively. The dwell time (time interval between successive 8-nm steps) of every other step in such a construct would be different if kinesin moved by hand-over-hand model but not if it did by inchworm models. The time course of the displacement produced by a single heterodimer was measured through optical trapping nanometry and showed steps with a long dwell time alternating with ones with a short dwell

time lending support to hand-over-hand mechanism [119]. Finally the step-wise motion of individual native and recombinant kinesin homodimers was measured at high spatiotemporal resolution, using an optical force-clamp apparatus [63, 64, 64]. It was found that the stepping rates and dwell times of the mutant can alternate between two different values at every other step, causing kinesin molecules to “limp”, indicating two distinct molecular configurations, thereby excluding fully symmetric models and suggesting that kinesin advances by some form of asymmetric hand-over-hand mechanism [62]. Yildiz developed a technique, Fluorescence Imaging One-Nanometer Accuracy (FIONA), that is capable of tracking the position of a single dye with nanometer accuracy and sub-second resolution [81]. Yildiz *et al.* have labeled a single head of the kinesin dimer with a Cy3 fluorophore and used FIONA to monitor position of the dye as the kinesin moved on microtubules. It was observed that a single kinesin heads take steps of 17.3 ± 3.3 nm but 8.2-nm steps. A kinetic analysis of the dwell times showed that the dwell-time histogram on which number of steps is plotted versus step-time duration is a convolution of two exponential processes suggesting that observed 17-nm steps alternate with 0-nm steps. These results strongly support asymmetric hand-over-hand mechanism [81] and are consistent with postulated conformational changes where the rear head passes the front head simultaneously with neck-linker warping and unwrapping around the stalk. Sideways drag slows the kinesin motor asymmetrically, which suggests left-right asymmetry to the forward-stepping motion [80, 55].

1.3.2 Mutations in Neck Linker result in impaired motility of Kinesin while the ATPase and MT binding remains undisturbed.

As mentioned before kinesin motor domains contain a catalytic core, which is conserved throughout the kinesin superfamily, followed by a neck region, which is conserved within subfamilies and has been implicated in controlling the direction of motion along a microtubule [66, 67]. It has been initially thought that the coiled coil domain must unwind at some stage to allow movement along microtubules [36, 15, 38], but experiments using hybrid kinesin with a very stable coiled coil argue against such models [21]. Deletion of neck coiled-coil [68] or neck hinge [69] regions results in an approximately five fold reduction of microtubule velocity while replacement of the neck linker with a designed random coil resulted in a 200500-fold decrease in microtubule velocity although ATPase rates were within order of magnitude from wild type levels. The catalytic core of kinesin, without any addi-

tional kinesin sequence, displayed microtubule stimulated ATPase activity and nucleotide-dependent microtubule binding suggesting that the catalytic core is sufficient for allosteric regulation of microtubule binding and ATPase activity and that the kinesin neck linker functions as a mechanical amplifier allowing to amplify conformational changes of ATP hydrolysis to stimulate a step [65]. Conformational changes in the linker when ncd binds to microtubules were first revealed using electron paramagnetic resonance (EPR) [76]. The free-energy changes associated with the neck linker conformational change, as determined by EPR, are favorable but small (≈ 3 kJ/mol). The large, favorable enthalpy changes balanced out by large unfavorable entropy changes indicate that the neck linker takes more structure upon MT binding, perhaps by interacting with the catalytic core and subsequently undocks and undergoes a transition into a high entropy state [77]. This conformational change requires both microtubules and a γ -phosphate in the active site [6, 7].

1.3.3 Neck Linker Plays Crucial Role in Motility

Upon those observations a model was built in which movement involves a transition from a disordered to an ordered state, with ATP binding providing the energy source for rectifying this Brownian ratchet with force generated upon ATP binding [21]. This could induce zippering of the neck linker, which would, in turn assist in dissociating the rear head [14, 22, 23] and displacing it by 16nm to the next available binding site producing rapid 8-nm steps [12]. This model also suggests that a backward load could slow down the motor [25] by adversely affecting the rate of neck linker docking and cause kinesin to take a backward step at stall loads [26] by reversing this process. A forward load could speed up movement [26] by inducing neck linker docking and/or by accelerating the dissociation of the rear head. The crystallographic investigations and cryo-electron microscopy was used to obtain low resolution three-dimensional maps of kinesin attached to microtubules *via* a single motor domain [35, 36]. The rear, unattached motor domain was found oriented towards the direction of movement. This was an important result, suggesting that the directionality of these motors might be determined by a region outside the motor domain core itself. The most likely candidate appeared to be the region linking the motor domain core and the stalk indicating that the neck linker can sense conformational changes at the ATP binding pocket situated on the other side of the core. This could be mediated by loops L4a, L10 and L13 since they connect to β -strands ($\beta 3$, $\beta 6$, $\beta 7$ and $\beta 8$, respectively) reaching into nucleotide binding pocket [121].

1.3.4 Changes in switch I and II due to ATP binding lead to zipper-like docking of NL

The study of the monomeric kinesin motor KIF1A combining X-ray crystallography and cryo-electron microscopy allows analysis of force-generating conformational changes at atomic resolution showing that similarly to other G proteins [123], in the ATP state in kinesin, both switch I and II regions become more structured by contacts with the microtubule and this interaction might be crucial for proper positioning of residues involved in ATP hydrolysis, which was further supported by mutational studies [77, 61]. Improved site specific EPR measurements showed that when microtubules are absent the neck linker exist in equilibrium between two structural states implying that the nucleotide binding does not control neck linker position. However, sulfate binding near the nucleotide can stabilize docked conformation of neck linker. The EPR signature of this state strongly resembles that seen in the microtubule-bound kinesin in complex with AMPPNP, suggesting a mechanism by which microtubule binding may activate the nucleotide-sensing mechanism of kinesin [124]. It has been proposed that $\alpha 4$ helix which is positioned at the end of switch II in the ADP- or nucleotide-free state, swings outward and downward, pushing the neck linker away from the catalytic core. In the ATP state, the $\alpha 4$ helix is brought closer to the nucleotide pocket, by interaction of neck-linker residues along the catalytic core [122, 91] allowing the neck linker to dock to the core. Recently physically motivated models of kinesin motor function have been developed within the framework of rectified Brownian motion since it allows in the most intuitive way to account for the directed motion arising from weakly favorable neck linker zippering. In those models rate limiting steps arise directly from the force-dependent inhibition of ATP binding to a microtubule head [125, 126]. Those models however don't have solid structural basis and the physical mechanism of kinesin motility remains uncertain and the exact mechanism of force generation remains yet to be determined.

1.4 Optical Trapping Technique

Although, as outlined above, kinesin has been extensively studied through bulk assays obtaining molecular description of how the kinesin motors functions greatly benefited from development of single molecule techniques especially optical force trap which yields quantitative information about mechanical forces involved in interactions at single molecule level [127]. The foundation for development of this technique was established by discovery

and experimental demonstration of radiation pressure [88]. The first experimental observation of single-beam gradient force radiation pressure particle trap to trap dielectric particles of various sizes demonstrated feasibility of this approach [128] and its application to biology. Initially fixed traps allowed to study motor-coated bead movement at low spatiotemporal resolution [48] but further advances especially the advent of commercially available three-dimensional piezoelectric stages with capacitive sensors has resulted in higher spatial precision and improved calibration of both forces and displacements [127]. Use of neodymium:yttrium-aluminium-grnet (Ny:YAG) and neodymium-yttrium-lithium-fluoride (Nd:YFL) lasers helped to decrease radiation damage and noise allowing work with fragile biological samples [127]. Sensitive position detectors, based on interferometry or quadrant photodiodes (QPDs) have been added to track bead position with subnanometer accuracy and high bandwidth. Faster and more precise steering of trapping beam has been achieved with computer-controlled galvanometer mirrors or acousto-optics deflectors [80]. Most recently optical tweezers have been integrated with single molecule fluorescence by alternately modulating the optical trap and excitation beams. In this way neither trap stiffness nor single molecule fluorescence sensitivity are compromised at high modulation frequencies allowing for study of real-time binding kinetics or energy transfer mechanisms [129].

This advances allowed study of intact cells and subcellular components such as viruses, bacteria, yeast, archaea eukaryotic cells and even individual organelles [89, 90] which allowed study for example of red blood cells [92], lymphocytes [93] and bacterial flagella. DNA and RNA properties [94, 95, 96, 97] and interactions with helicases [98, 99], exonucleases [100] and translocases [101] and viral packing proteins [102]. Optical tweezers were also instrumental in study of polymers such as microtubules [103] and actin filaments [104] and protein folding to visualize mechanical unfolding [105, 106]. Finally mechanochemical cycle of motor proteins, beyond kinesins, such as dynein [107], myosin II [108], myosin V [109] and myosin VI [110] have been extensively studied. The major disadvantage of the use of optical tweezers in biology is radiation damage to the sample which are not fully negligible and may alter the activity of the protein. Also light absorption by the buffer solution or by a trapped bead can increase the temperature around the sample and create convection currents [111, 112]. Optical tweezers experiments also advanced cold-atom manipulations [113] and allowed for the attainment of Bose-Einstein condensation [114], development of atom lasers [115] and practical advances in atomic clocks and measurements of gravitational forces and induced space time curvatures [116].

Chapter 2

Proposed Mechanism of Kinesin Motility

Together with the dimer structures, work on hybrid and mutant motors has led to remarkable progress over the past three years. For conventional kinesin, the linker regions immediately adjacent to the motor domains have been shown to determine the direction and speed of movement along microtubules and indicated that this region is intimately involved in the molecular mechanisms of kinesin motility. However specific atomistic details of interactions with the core that make neck linker sensitive to subtle changes at the distant nucleotide binding pocket and allow for force transmission and generation are unknown.

2.1 Structural Analysis

Available monomeric kinesin structures in ADP state (1BG2 citeSindelar2002) with unbound neck linker (NL) and ATP state-like states with NL bound to the motor head (1MKJ [124], 2KIN [34]) share 86.2% sequence identity and are structurally very similar as their root mean square deviation of their backbone is less than 0.8 Å. NL contains two β strands $\beta 9$ and $\beta 10$ (Figure 2.1).

In the ATP-bound state $\beta 9$ interacts mainly with cover strand by forming a β -sheet and through I327 with NL. In the ADP state CS is separated from the motor head core and is unstructured which leaves NL and the motor head interacting through a hydrogen bond between G77 and N334 (highly conserved residue [130] between $\beta 9$ and $\beta 10$) and between S225 and N334. In this confirmation $\beta 10$ forms a short stretch of β -sheet with $\beta 7$ on the motor

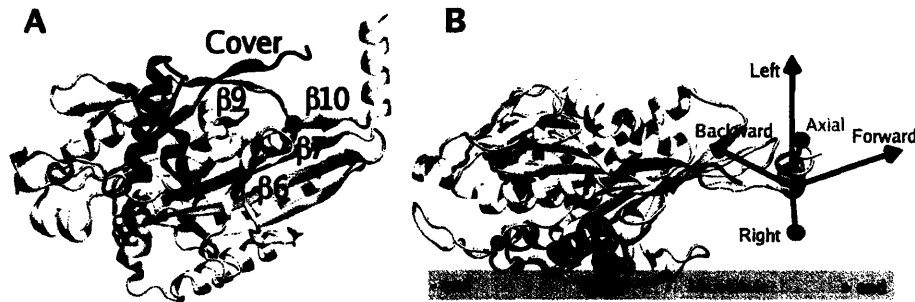


Figure 2.1: Role of NL in motility. Figure adopted from [131]. A. Structure of motor domain (2KIN) with structural elements important for the movement generation hypothesis highlighted. B. Setup for the molecular dynamics simulation where force was applied to kinesin in an attempt to simulate walking under load conditions. Brown spheres are the immobilized residues. Point of force application is shown along with pulling directions

head [131]. This lack of strong binding interaction between NL indicates that affinity-driven zippering initiated by insertion of I327 into the binding pocket, which would in turn trigger docking of rest of the NL [91] is unlikely due to weak interactions between those regions. Moreover binding partners for the rest of NL have almost the same conformation at both the ATP and ADP state.

2.2 Molecular Dynamics Simulation

In a MD simulation performed by Wonmunk *et al.* where C_{α} atoms which are expected to interact with microtubules were constrained as anchors (Figure 3) to mimic MT-bound state it took 440-480pN force to mechanically unbind NL during the 0.4-0.8ns simulation time scale. Once the unbinding was initiated it proceeded by a rapid initial release of $\beta 10$, leading to intermediate state in which N334 is held in place, followed by a release of $\beta 9$. This agrees with the above analysis: N334 acts as a latch that hold NL in a constrained state and the force to break that bonds is 440-480pN. Once this bond is broken, the $\beta 9$ part of NL unbinds rapidly since there are no strong interactions to hold it in place. After the full unbinding of NL, no further unfolding of the protein occurred until the end of simulation suggesting that the motor head has stably formed citeWonmunkMAN.

Subsequently neck helix that is a part of the neck coiled-coil stalk was constrained and the motion of the freely moving motor head to see the role of NL in controlling the head motion, which is analogous to the situation in which an unbound motor head is performing a "diffusive search" for the next binding site, with the neck coiled-coil being less mobile. This revealed that the position and orientation of the motor head fluctuate more when CNB is not formed than when CNB is present [131].

This results indicated that CNB may be responsible for generating the force for a walking stroke. This scenario was tested by running MD simulation with the same atoms constrained as in the previous one and letting the motor interact freely with MT. For 1MKJ and 2KIN, rebinding-like events of NL were indeed observed and in both cases CNB bent towards the binding pocket, but the ASN latch and $\beta 10$ did not form bonds with the residues on the motor head which were postulated to be binding partners. Through the simulations in which the unbound motor head moved, re-binding of CNB occurred, which suggests that once the motion of CNB toward the binding pocket is initiated, it is largely independent of the rest of the motor head [131]. It was interesting to notice that in this simulation L13 protrudes and interferes with the binding of neck linker and experimentally, the G291A/G292A mutation in L13 which should reduce the flexibility of L13 and increase sterically blocking of the tight binding of the neck linker led to 100 fold decrease in MT gliding velocity [65]. The autonomy of the conformational bias of CNB was confirmed by running explicit-water simulations of isolated CNBs with the motor domain deleted and the base of CNB fixed in space [131]. This results indicated that power stroke generation is a local property of CNB, rather than the global conformational change of the motor head. The force map generated during this simulation is anisotropic in the transverse direction such the left side of the direction of kinesin movement has more populated low force field. This is consistent with the two-dimensional force clamp experiment in which leftward force caused a greater decrease in walking velocity than rightward force. The stall force F_s , defined in this case as the force required to prevent binding and subsequent docking of CNB was estimated to be $F_s = 150pN$ [131], which however cannot be directly compared with experimental results but is consistent with them.

. Structural data and molecular dynamics simulations indicate that CNB, consisting of a β -sheet made up of CS and the first half of the NL is the force generating mechanism in kinesin motility that is also responsible for direction of movement. The conformational bias of CNB appears to be primarily enthalpic, suggesting that its hinge-like motion is a power stroke.

2.3 Proposed Mechanism for Kinesin Motility

When the trailing head detaches from MT upon release of phosphate CS on both ends are separated from the unbound and flexible NL. The reduced strain on NL of the leading head allows ATP binding, which leads to CNB formation and a power stroke, because in this conformation switch II is close to $\alpha 6$, preventing the formation of its extra helical turn. The unwound portion of $\alpha 6$, which connects directly to $\beta 9$, renders $\beta 9$ out of register with CS, blocking CNB formation. When ATP binds, switch II, retracts, allowing the extra helical turn of $\alpha 6$ to form. CS and $\beta 9$ are now in register so they can form CNB, leading to the power stroke. After the power stroke the new leading head performs a diffusive search for the next MT binding site in a narrowly defined region rather than entire 16nm interval. During that time specific binding of ASN latch and $\beta 10$ to the motor head will be established, which would in turn assist in correct positioning of the leading head to make a step [131].

Chapter 3

Experimental Design

The proposed mechanism of kinesin motility is consistent with available mutagenesis studies of chimeras in which the neck domains were interchanged [8, 9, 10, 130], two dimensional force clamp experiments and stall force measurements [80], indirect measurements of moment of the arm [62], observed substeps in kinesin motion [141, 142], cross-linking studies [132], mutagenesis studies in which speed and stall force was measured [77] and evolutionary analysis [130]. However the stochastic nature of the pulling simulation made it difficult to find a clear correlation between the unbinding time and the direction of the pulling force. Moreover although CNB bent towards the binding pocket the ASN latch and $\beta 10$ did not form bonds with their partners and the motor head within simulation time within the simulation time. High simulation temperature (360K) caused deformations to parts of the the molecule.

Although the model is supported There were no studies up to date that would directly investigate the role of CS, NL or CSB formation therefore the proposed role of CNB in the kinesin motor requires experimental testing. Measurements and comparison of stall forces, velocities at various loads, processivity and step size between the wild type and mutant kinesin in which NL region or CS are mutated leading to limited or no CNB formation and hence to impaired movement.

3.1 Protein Engineering

3.1.1 Mutant Design

Four mutants where designed based on the *Drosophila* (for neck linker sequence see Table 1). The first mutant was designed to have entire neck



Figure 3.1: The structure of the motor head 2KIN targeted for mutations. Cover strand is shown in blue, P-loop is in green, $\alpha 3$ is red, Switch II region composed of $\alpha 4$ and L12 is yellow, $\alpha 6$ is colored violet and light violet and is connected to it neck linker. The amino acids targeted in mutaton are shown. First mutation removes entire neck linker, second one alters SER12 and ILE13 (in dark red) to GLY. In second mutation A9 and D11 are mutated to glycines (in dark blue) and finally A9G and D11G (in blue), SER12 (red) and E10 (in yellow) are mutated to GLY

linker cleaved (Aa1-12) and since the NL is deleted this mutant is expected to not be able to form CNB and hence not move. Second mutant has two point mutations (S12G and I13G) making the CNB formation unlikely as the main interaction amino acids are mutated or, if the CNB forms, the generated force is expected to be lower since the hinge region is more flexible. The third mutant has A9G and D11G mutation which are expected to obstruct the formation of CNB by decreasing NL and CS interactions and hence produce slower moving kinesins with lower stall forces. The last, fourth mutant, has A9G, E10G, D11G, D12G which is expected to completely prevent CNB formation rendering motion impossible (for quick reference about the mutants see table 2).

1	2	3	4	5	6	7	8	9	10	11	12	13	14	15	16
ATG	TCC	GCG	GAA	CGA	GAG	ATT	CCC	GCC	GAG	GAC	AGC	ATC	AAA	GTG	GTC
M	S	A	E	R	E	I	P	A	E	D	S	I	K	V	V

3.1.2 Cloning

The native *ncd* protein of *Drosophila* kinesin was expressed with a HIS tag from K410-BIO-HIS6 plasmid (generous gift from Jeff Gelles). Mutants 2-4 were generated using QuickChange mutagenesis (Stratagene, LaJolla, CA) with the appropriate primers. PCR amplification was performed using a proofreading DNA polymerase (Pfu polymerase, Stratagene, LaJolla, CA) in order to reduce the possibility of misincorporations. Mutant 1 was generated by synthesizing gene fragment from a series of primers and amplified by the polymerase chain reaction (PCR). The PCR product was isolated by agarose electropress and cloned into *XbaI* and *NgoMIV* (New England Biolabs) site of K410-BIO-HIS6. Colonies with appropriate inserts in correct orientation were obtained by extracting DNA from all available colonies and sequencing it with appropriate primers at MIT Biopolymer Facility (MIT). Each kinesin gene has its own ribosome binding site, and the two genes are flanked by a T7 promoter and a T7 terminator. All constructs were verified by DNA sequencing.

3.1.3 Protein Expression and Purification

BL21 *Escherichia coli* cells [9] containing the gene for T7 RNA polymerase under control of the *lac* operator were transformed K401-BIO-HIS or mutant DNA and used for expression of native or mutant *ncd* protein. Cells were grown with shaking at 37°C in LB media (10g of tryptone, 5 g of yeast extract, and 10g NaCl per liter) supplemented with ampicillin (100

$\mu\text{g/ml}$) and chloramphenicol (25 $\mu\text{g/ml}$). Overnight cultures of 25 ml were diluted into 500mL of fresh TB media (12g Tryptone, 24g Yeast Extract, 4ml Glycerol, 2.3 g Potassium Phosphate (monobasic), 12.5 g Potassium Phosphate (bibasic) per liter), incubated for around 3h to an absorbance of 0.53-0.60 at 600 nm and induced by addition of IPTG to 0.05 mM. After an additional 2h rifampicin was added (2 $\mu\text{M/l}$). After 10 h of incubation at 22^o , the cell were chilled and collected by centrifugation at 5,000g for 10 min. Cells were resuspended in 5mL of cold lysozyme buffer (20mM imidazole of pH7, 4mM MgCl₂, β mercaptoethanol 10mM, PMSF (Sigma P7626) 20 μM , 2 μM pepstatin (Sigma P4265), 20 μM TPCK (Sigma T4376), 20 μM TAME (Sigma T4626), 2 μM leupeptin (Sigma L9875), 20 μM soybean (Type-I, Sigma T9003)) and incubated at the shaker on ice for at least 30min in order for internal lysosome to degrade cell wall. The cells were lysed and the DNA/RNA fragmented by brief freezing and thawing cycles and subsequent addition of 0.5mg/ml of DNase (Grade II, Boehringer 104 159) and 1 mg/ml RNase (Type II-A, Sigma R 5000). Immediately after lysis the lysate was centrifuged (21,800g for 20 min) to remove insoluble material and the supernatant was centrifuged at 180000g for 30min. subsequent steps were performed at 4^oC, and all solutions were supplemented with ATP at 10 pM. The supernatant was mixed with Ni resin (Quiagen Ni-NTA Superflow) according to manufacturer instructions and incubated overnight. Protein was purified by Ni column by elution with increasing concentrations of imidazole and stored at -80^o in cryoprotectant solution (60% w/w sucrose, 2mM DTT, 50nM ATP) 35% w/v.

3.1.4 Microtubule Preparation

The tubulin (purified bovine brain tubulin; Cytoskeleton) was stored at -80 °C after fast freezing with liquid nitrogen was spun down (10000g, 30min, 4^o) and resuspended 28% v/v in polymerization buffer (79.3mM Pipes (Sigma P1851), 1mM EGTA (Sigma E-4378), 4.82mM MgCl₂ (Mallinckrodt H590), 1mM GTP, 0.14% v/v DMSO (Sigma D-5879) at pH of 6.9) and allowed to polymerize for 30min at 37^o. After this time polymerization is quenched by addition of 9% v/v of stop solution (55.2 mM Pipes (Sigma P1851), 0.68 mM EGTA (Sigma E-4378), 2.72 nM MgCl₂ (Mallinckrodt H590), 1mM GTP (Cytoskeleton BST06), 6 g/L NaN₃ (Sigma S-8032), 0.25mM Taxol (Cytoskeleton TXD01), 10% v/v DMSO (Sigma D-8579) at pH of 6.9) and stored at room temperature.

3.1.5 Bead Assay

Motility assays were performed following [117] by mixing , 0.8 or 0.44- μm -diameter silica beads were mixed with native kinesin [purified from as described above] at sufficiently low concentration such that fewer than one kinesin molecule, on average, was bound to each bead. Kinesin bead incubations were performed for 1h in a buffer containing 80mM Pipes (pH 6.9, Sigma P1851), 50mM potassium acetate, 4mM MgCl_2 (Mallinckrodt H590), 2mM DTT, 1mM EGTA (Sigma E-4378), 7M Taxol (Cytoskeleton TXD01), 100 $\mu\text{g}/\text{ml}$ casein as a blocking protein at saturating ATP concentration. An oxygen-scavenging system (250gml1 glucose oxidase, 30gml1 catalase, 4.5mgml1 glucose) was added to the kinesin-beads just before measurement. Beads were optically trapped and held near microtubules that had been immobilized on a polylysine-coated glass cover slip and washed with taxol containing buffer.

3.2 Optical Trapping

An optical trap is formed by tightly focusing a laser beam with an objective lens of high numerical aperture NA where $NA = n \sin \theta$ where n is an index of refraction and θ is half-angle of the maximum cone of light that can enter or exit the lens [118]. A dielectric particle near the focus will experience a force due to the transfer of momentum from the scattering of incident photons. The force produced by such a trap can be decomposed into a scattering force, in the direction of light propagation and a gradient force in the direction of the spatial light gradient. If there is a steep intensity gradient such as near the focus of the laser the gradient force becomes significant. The gradient force arises from the fact that a dipole in an inhomogeneous electric field experiences a force in the direction of the gradient. In an optical trap, the laser induces fluctuating dipoles in the dielectric particle, and it is the interaction of these dipoles with the inhomogeneous electric field at the focus that gives rise to the gradient trapping force. For stable trapping of a particle located slightly beyond focal point the axial gradient component of the force pulling the particle towards the focal region must exceed scattering component pushing it away from that region. For small displacements ($\approx 150\text{nm}$), the gradient restoring force is simply proportional to the offset from the equilibrium position i.e. the optical trap acts as Hookean spring whose characteristics stiffness is proportional to the light intensity (laser power) [127].

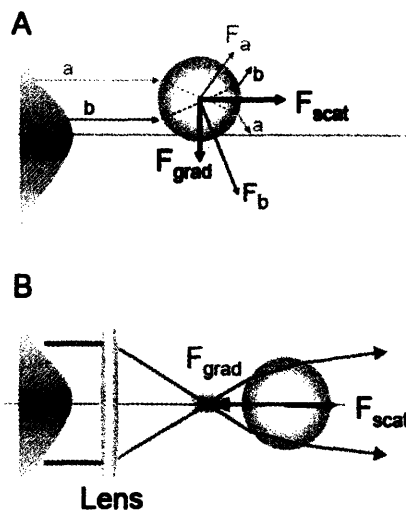


Figure 3.2: Forces acting on dielectric sphere. A. under the influence of simple Gaussian laser beam where F_{grad} and F_{scat} are of similar magnitude. B. In case of focused laser or optical tweezers where F_{scat} dominates. Figure taken from [143]

3.2.1 Trap Design

The trap is modeled after previously described arrangement [80, 129] based on an inverted microscope (Eclipse TE200; Nikon Instruments Inc., Melville, NY) and combines lasers for optical trapping (1064nm; Coherent, Santa Clara, CA), position detection (975 nm; Corning Laserton, Bedford MA). The detection arrangements consist of a pair of computer controlled acousto-optic deflectors (AODs; IntraAction, Bellewood, IL) which allow for computer steering of the trapping beam. Both, the trap and detector wavelengths were selected to minimize photodamage [80, 127] and were guided into the microscope objective (100 \times , 1.40 numerical aperture, oil infared, Nikon, Melville, NY) via a dichroic mirror (Chroma Technology, Rockingham VT) that reflects only near-infrared light. The diameter of the trapping laser beam is adjusted with a telescope to slightly overfill the objective pupil to ensure high-efficiency trapping because it increases the ratio of trapping to scattering force. After passing through the microscope condenser lens, the detection beam is spectrally isolated (Andover, Salem, NH) from the trapping beam and imaged on a position-sensitive device (PSD; Pacific Silicon, Westlake, Virginia, CA) for back focal plan detection. Custom software written in LabView (LabView; National Instruments, Austin, TX) acquired all signals through a 16-bit A/D board (National Instruments) and automated instrument operation enabling it to be computer controlled.

3.2.2 Position Calibration

Initial calibration of the motion of the trap itself in the specimen plane against beam deflection, using AODs. Position determination using a movable trap was performed by moving a trapped bead through the detector area in a raster pattern to cover the entire active area region of the sensor and recording the position signal. Voltage to nanometer conversion of the QPD directly from the power spectrum of the trapped bead is performed by directly mapping the voltage response to QPD movement through 5th order fitting. This calibration method offers several advantages, main one, being that position calibration can be performed individually for each bead, which eliminates errors arising from differences between beads (estimated to be 5% coefficient of variation in diameter [127]) and because the calibration and detection with dual beam takes place in the same axial plane, calibration errors arising from the slight axial dependence of the lateral position signals are avoided. This calibration is performed automatically by LabView software controlled scanning and it has been shown to agree to within $\approx 20\%$

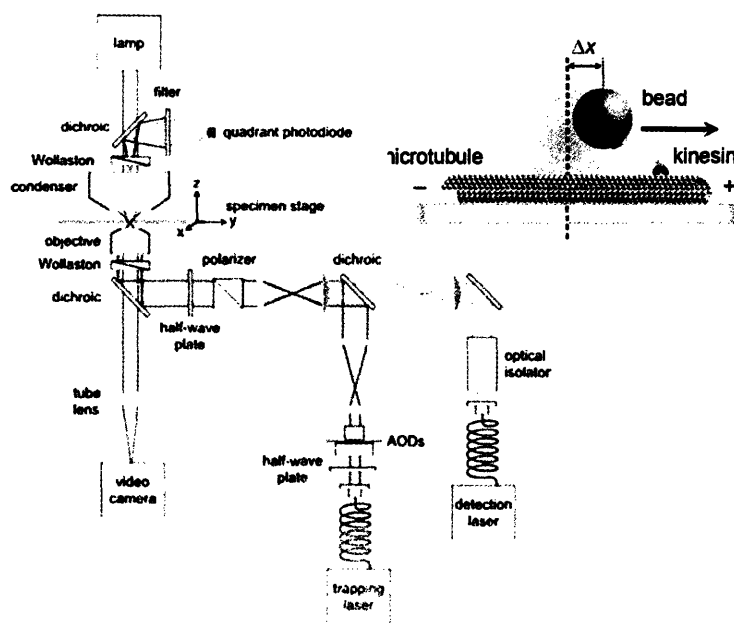


Figure 3.3: A. Trap design showing major structural components: trapping laser, AODs, detection laser and QPD. Figure adapted from [129]. B. Cartoon showing bead with kinesin attached to it trapped in the laser beam. Figure taken from [144]

of the sensitivity as measured by more direct means [127].

3.2.3 Stiffness Calibration

Stiffness calibration was performed based on thermal fluctuations of a trapped bead through the equipartition theorem which states that every degree of freedom in a harmonic potential contains $\frac{1}{2}k_B T$ of energy. This was used to relate measurement of the instantaneous displacement of a trapped particle to the available energy of the system defined as:

$$\frac{1}{2}k_B T = \frac{1}{2}k \langle (x - x_{eq})^2 \rangle \quad (3.1)$$

where k_B is Boltzmann's constant, T is absolute temperature and x is the displacement of the trapped bead from the equilibrium position x_{eq} . Thus, by measuring the positional variation of the trapped bead $\langle \delta x^2 \rangle$ which equals the integral of the position power spectrum recorded by calibrated detector. The primary advantage of this method is that it does not depend explicitly on the viscous drag of the trapped particle. Care has to be taken during calibration since any added noise and drift in position measurement serve only to increase the overall variance, thereby decreasing the apparent stiffness estimate. The trap was calibrated as described and shown to deliver sufficient power to be capable of trapping 800nm radius polystyrene beads with a stiffness of ≈ 0.1 pN/nm per 100mW of power.

3.2.4 Trapping Assays

Measurements of displacement were made by using an optical force tweezers apparatus using either $0.80\mu\text{m}$ or $0.44\mu\text{m}$ diameter beads. Each kinesin molecule was put on 3 different microtubules and if it didn't show any movement on any of them it was assumed that this bead would not move. To ensure work in the single molecule regime, data only from assays in which fewer than half the tested beads moved were analyzed.

Chapter 4

Unloaded Velocity Measurements

4.1 Data Acquisition and Analysis

Bead assay was prepared for purified and mutant kinesin as described above and tested by the standard optical trapping setup described above. The movement was visualized by sub-pixel resolution video taken from microscope bright-field image.

The stack of camera images is read into MATLAB (Mathworks) code which is a modification of IDL Tracking Software of Digital Video Microscopy [135]. Those images suffer from geometric distortion, nonuniform contrast, and noise mostly due to digitization and uneven illumination so initially the background is modeled as a boxcar average and subtracted. Subsequently particles are identified as Gaussian-like distributions of brightness on a dark background and the brightest one is chosen to be the bead of interest. This bead is approximated by a centroid and tracked. Once this bead is found in a sequence of video images the location in each image is matched with corresponding locations in later images to produce a trajectory. After visual examination of the trajectory and the video sections of the video corresponding to the processive movement along the microtubule are separated and from trajectories of movement within those sections velocity of movement is calculated.

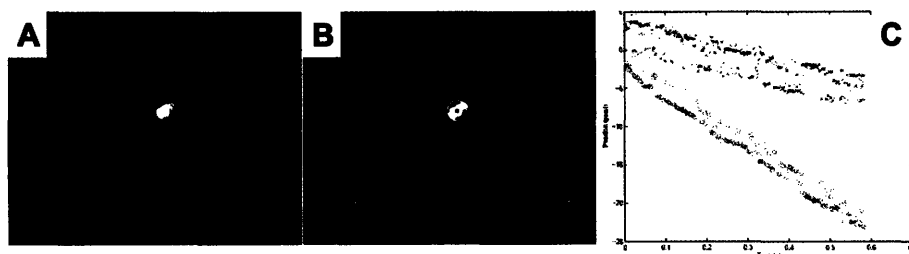


Figure 4.1: Schematics of the steps of the algorithm used to extract velocities from video records. A. Raw data image B. Data image after centroid finding and background Rosin thresholding C. x and y -position traces extracted from a movie.

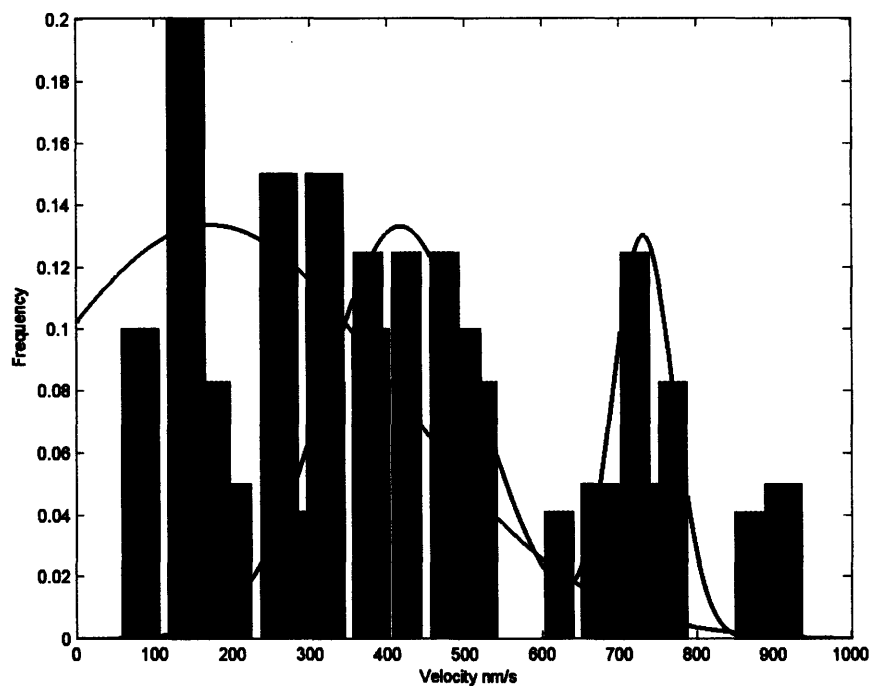


Figure 4.2: Histogram of unloaded velocities obtained from video measurements for mutant (blue) and wild type (red) kinesin constructs. In general, mutant's unloaded velocities are significantly smaller than those of wild type.

4.2 Results

This mutant of *Drosophila* has A9G and D11G which are thought to impede cover neck bundle formation by decreasing number of interactions between cover strand and neck linker. This relatively minor change cause visible change in the unloaded velocity. The normalized histogram of unloaded velocities for both wild type and A9G, D11G mutant is shown on Figure 4.2. The average velocity of the mutant kinesin is 173 nm/s with a relatively wide distribution ($\sigma=235\text{nm/s}$)The distribution of wild type kinesin is bimodal with the first peak at 417nm/s ($\sigma=97\text{nm/s}$) and the second one at 731nm/s ($\sigma=39\text{nm/s}$). The second peak of wild type distribution is consistent with previous studies [92, 136]. Those studies don't show the significant distribution of slower moving wild type kinesins due to the fact that in those studies recordings would only be collected if kinesin exceeded velocity of 400nm/s. The mutant moves significantly slower and almost never reaches wild type velocities indicating that motility of the molecule was impeded by the mutation.

Chapter 5

Loaded Velocity Measurements

5.1 Data Acquisition and Analysis

Bead assay was prepared for purified and mutant kinesin as described above and tested by the standard optical trapping setup described above. Data were collected when the bead was observed to move forward and snap back when trapped and positioned on microtubule.

Collected raw voltages were first converted to position using position calibration described above. Subsequently the scatter plot of bead displacement is fitted in order to find the orientation of microtubule and adjust the displacement with respect to that orientation. Finally stiffness calibration outlined above allows to convert this displacements to force. Calibrated data segments are filter using moving window averaging with small size window in order to remove high frequency noise and then smoothed with Savitsky-Golay filter [137]. Peaks above a certain specified threshold are isolated and the beginning of each peak is found using an algorithm similar to Rosin thresholding [138] and the portion of the peak representing a snap-back is removed. Peaks for further analysis are selected based on the following criteria: (1) the time between the beginning and the beginning of the snap-back must be longer than 0.3s (2) The relative height of the peak from the base to the pinnacle is above specified value (3) The absolute height from the zero to the pinnacle must reach certain specified value (4) The duration of the peak has to be shorter than 3s (4) Peak must not have backward steps larger than 9nm. All thresholds are set by hand for each bead separately

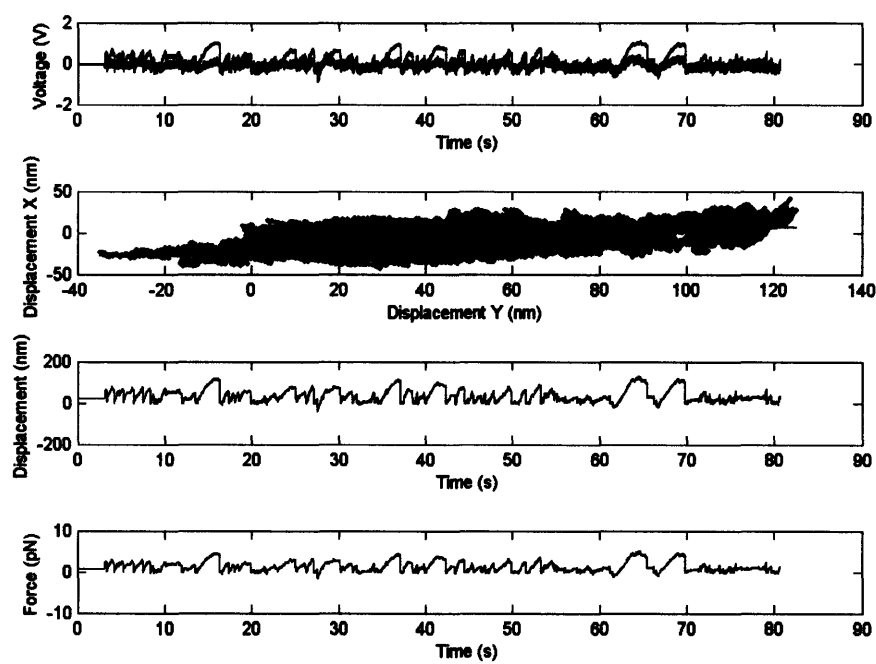


Figure 5.1: Sample record. A. Raw voltages in x (red) and y -direction. Steps and stalling of molecule at high forces can be clearly seen. B. Scatter plot of kinesin positions and found microtubule alignment C. Displacement corrected for microtubule orientation D. Force obtained by calibration of displacement.

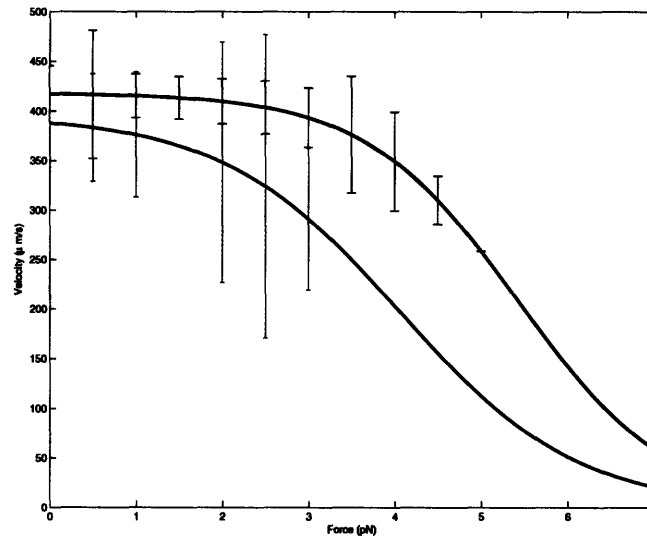
after a visual analysis of calibrated data. Selected peaks of position and force are fitted with cubic splines and the velocity is measured by numerical differentiation of the position spectrum at specified force. The average and maximum values for each bead are calculated from Gaussian fits as the data were normally distributed and collected for all the runs. Moreover values for all the beads are collected and fitted with a simple force-velocity relationship widely used for many mechanoenzymes [140, 139]:

$$v(F) = \frac{v_{max}}{1 + \exp\left[\frac{(F-F_{1/2})\delta}{k_B T}\right]} \quad (5.1)$$

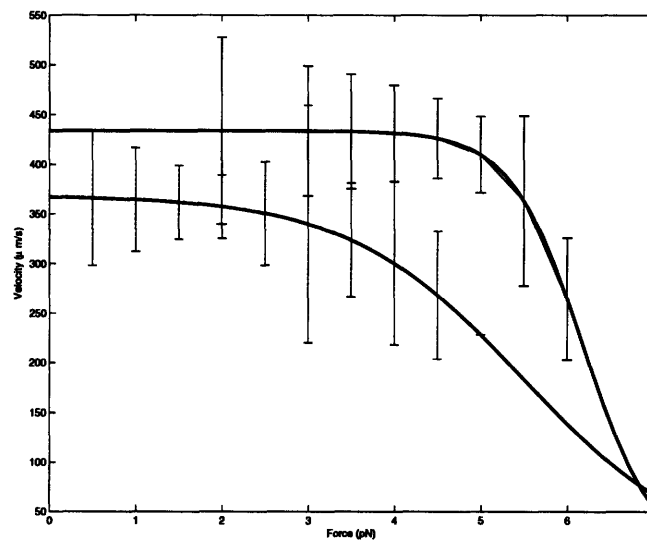
where v_{max} is the unloaded velocity, $F_{1/2}$ is the force at which the velocity reaches half its maximal value, k_B is Boltzman's constant, T is the temperature, and δ is a parameter that represents the effective distance over which a force acts and forced through zero at $F=7.2\text{pN}$, which is the literature value for kinesin stall force [136]. In the power stroke model δ represents the distance from the pre-translocate position to the transition state. The error bars represent standard error on the mean $S_E = \frac{\sigma}{\sqrt{(n)}}$ where σ is an estimate of the standard deviation of the population and n is the number of counts.

5.2 Results

The force velocity curves were measure for mutant kinesin (A9G and D11G) and wild type one attached to two different size beads. Figure 5.2 A shows comparison of the force velocity curves for mutant and wild type kinesin attached to $0.8\mu\text{m}$ beads and Figure 5.2 B to $0.44\mu\text{m}$. In both cases the same simple force-velocity relationship was used to fit the results. In the case of $0.8\mu\text{m}$ beads unloaded velocity of wild type kinesin ($F=0$) is 420 nm/s while for mutant it is slightly lower 380 nm/s . In the case of $0.44\mu\text{m}$ beads the unloaded velocity for wild type kinesin was very similar (430 nm/s) to the one obtained using $0.8\mu\text{m}$ beads and the velocity of the mutant was also lower (370nm/s). In both cases at all the loads the velocity of the mutant follows the general trend of the velocities for wild type but is consistently slower. The data taken with $0.44\mu\text{m}$ beads show sharper drop down then the ones at $0.8\mu\text{m}$ which is likely due to the fact that the force is applied more directly with the smaller beads and bead rotation or force tangential to the axis of movement are less likely. The predicted velocities are slightly lower but in general agreement with published values [92, 136] while the mutant is



(a)



(b)

Figure 5.2: Force velocity curves. A. Force velocity curve for wild type (red) and mutant (blue) kinesin obtained from experiments with $0.8\mu\text{m}$ beads. Although velocities are lower than generally acknowledged it can be clearly seen that mutant is visibly slower than wild type at all forces. B. Force velocity curve for wild type (red) and mutant (blue) kinesin obtained from experiments with $0.44\mu\text{m}$ beads. Although velocities are still lower than generally acknowledged, mutant is slower than wild type at all forces.

slower likely due to impeded CNB formation increasing dwell times between the steps especially at higher forces.

Chapter 6

Stall Force Measurements

6.1 Data Acquisition and Analysis

Bead assay was prepared for purified and mutant kinesin as described above and tested by the standard optical trapping setup described above. Data were collected when the bead was observed to move forward and snap back when trapped and positioned on microtubule.

Collected raw voltages were converted to force as previously described. Subsequently peaks were using moving window averaging with small size window in order to remove high frequency noise and then smoothed with Savitsky-Golay filter [137]. Peaks for further analysis are selected based on the following criteria: (1) the time between the beginning and the beginning of the snap-back must be longer than 0.3s (2) The peak reaches above baseline threshold (3) The duration of the peak has to be shorter than 3s. All thresholds are set by hand for each bead separately after a visual analysis of calibrated data. The pinnacle of each peak was taken as the stall force for a given peak. The peak heights were collected for all runs for mutant and wild type kinesin.

6.2 Results

The normalized histogram of stall forces for both wild type and A9G, D11G mutant is shown on Figure 6.1 and can be reasonably fitted with the Gaussian distribution. The data represent cumulative findings from $0.8\mu\text{m}$ and $0.44\mu\text{m}$. The average stall force for the wild type kinesin is 2.8 pN but forces reach 6 or 7pN matching the reported stall forces [92]. The mutant force distribution is significantly shifted to left with the average force of 1.6pN. None

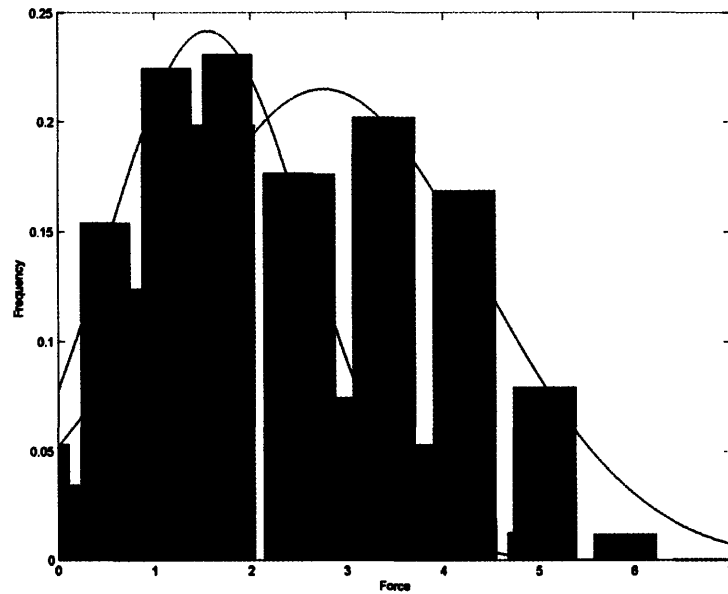


Figure 6.1: Histogram of stall forces presenting the distribution of stall forces for wild type kinesin construct (red) and mutant (blue). Wild type stall force is around 2.8pN, which although lower than found by [80] is significantly higher than 1.6pN for mutant kinesin

of the mutant molecules reached stall forces above 5pN, showing that the impaired power stroke mechanism decreases the force of the power stroke. Moreover the mutant force distribution is much tighter with a standard deviation $\sigma = 1.0$ as compared to $\sigma = 1.6$ for a wild type indicating that the mutant has much lower range of operating velocities.

Chapter 7

Processivity

7.1 Data Acquisition and Analysis

Bead assay at single molecule level was prepared for purified and mutant kinesin as described above and tested by the standard optical trapping setup described above. The movement was visualized by sub-pixel resolution video taken from microscope bright-field image.

The stack of camera images on which the bead is moving processively from the time it is bound to the microtubule and the time it dissociates from the tube is read into MATLAB (Mathworks) and particles were tracked as described before. From the trajectories the time corresponding to the processive movement along the microtubule (processivity) is measure.

7.2 Results

The normalized histogram of processivity for both wild type and A9G, D11G mutant is shown on Figure 7.1, however due to small number of counts available it was impossible to determine what distribution the data follows and subsequently they were not fitted with any functional form. However it is evident that mutant molecules are much more processive than wild type. While the processivity of wild type kinesin varies between 2-11s with occasional more processive molecules staying bound to microtubule for as long as 16 or 20s, processivity of the mutant kinesin varies between 17-28s. The ultraprocessivity of mutant kinesin may arise from the fact that while the power stroke mechanism is being the microtubule binding is stronger and dissociation more rare as mutant has increased flexibility hence making binding to microtubule easier.

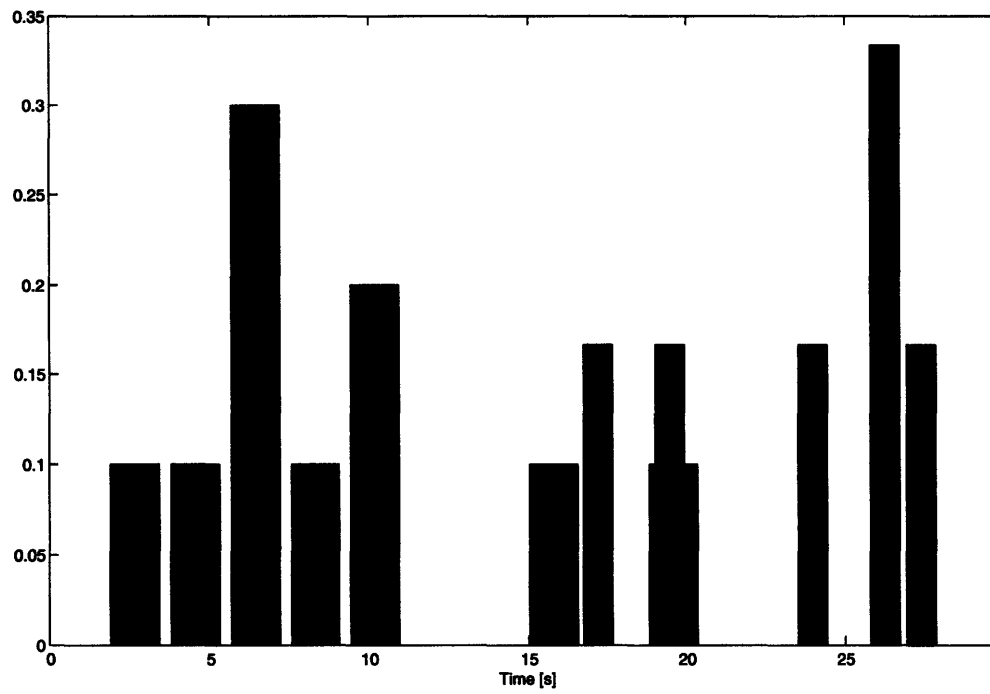


Figure 7.1: Histogram of length of processive motion for wild type kinesin construct (red) and mutant (blue). Mutant kinesin is much more processive than wild type molecule.

Chapter 8

Stepping Characteristics

8.1 Data Acquisition and Analysis

Bead assay was prepared for purified and mutant kinesin as described above and tested by the standard optical trapping setup described above. Data were collected when the bead was observed to move forward and snap back when trapped and positioned on microtubule.

Collected raw voltages were converted to force as previously described. Kinesin steps were isolated from the data using t -test based algorithm on unsmoothed data. For each data point 80 ms of samples before and after that sample were compared by the t -test. The resulting t -value profile versus time showed upward spikes for forward steps and downward spikes for snap-backs and backward steps. Absolute t -values above a defined threshold were scored as steps, and the peak t -value time coordinate was defined as time zero for the given step. The threshold was found by Rosin thresholding of a peak t -values. Subsequently the step height was calculated by taking the average of the points before and after the step and calculating the distance between them.

Backwards steps were found by visual analysis of the calibrated position data and counted for all records. Only steps that were preceded and followed by a brief period of no displacement were counted to discount the backwards steps arising from snap-backs.

8.2 Results

Distribution of step sizes for both mutant (A9G, D11G) and wild type was obtained as described above and is shown on Figure 8.1. Mutant and wild

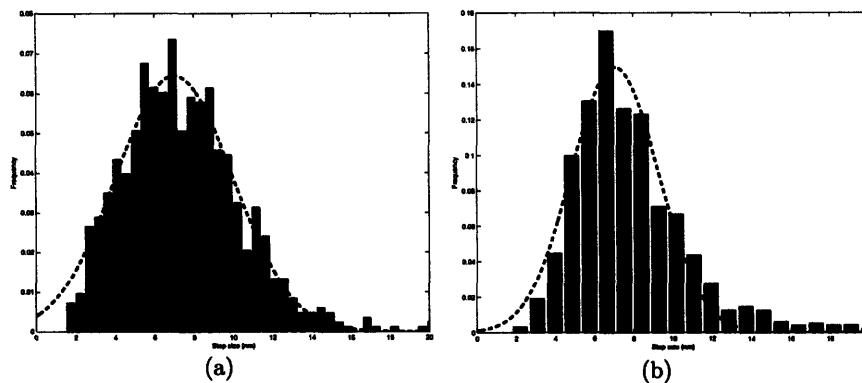


Figure 8.1: Histogram of step sizes for A. wild type with average step size of 7.8nm B. Mutant construct with smaller average step size of 7.1nm

type results from experiments with $0.8\mu\text{m}$ and $0.44\mu\text{m}$ were added as they looked very similar. The distributions for wild type and mutant have very similar mean for wild type $\approx 7.8\text{nm}$ and mutant $\approx 7.1\text{nm}$. This indicates that the step size is not affected by mutation in cover strand. The step size is smaller than the reported 8.2nm [80] most likely due to the fact that when the points are averaged before and after the step some of the upward and downward going step slope is included decreasing the step size. The distributions have very similar standard deviation (wild type $\sigma=2.97$ and mutant $\sigma=2.22$) further reinforcing the notion that the stepping itself was not affected.

The wild type kinesin had approximately 5% of backwards steps which is consistent with results reported in the literature [80, 136], while mutant molecule showed significantly higher percentage of mutant steps 10% which, although still within estimated range for kinesin is on the very end of the possible range (5%-10%) [80] indicating that the directionality mechanism can be affected by the mutation.

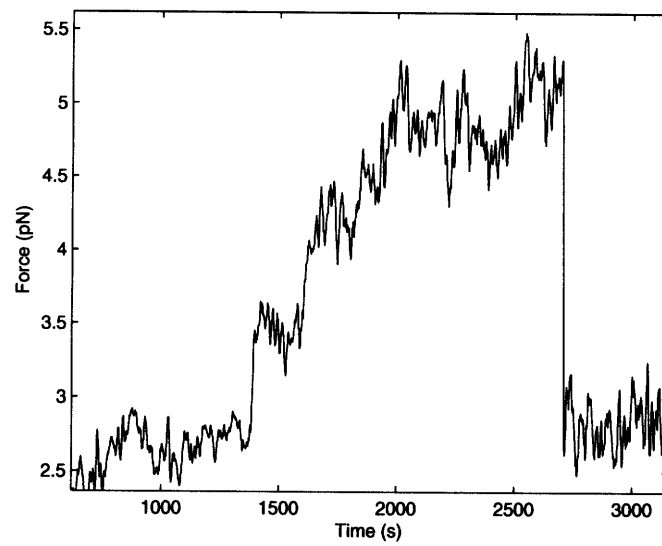


Figure 8.2: Sample record of kinesin walking against increasing force. Clear steps can be seen on the rising slope

Chapter 9

Conclusions and Future Work

Motility of the kinesin motor has been a subject of intensive studies for over a decade. Work on hybrid and mutant motors as well as availability of crystal structures has led to remarkable progress over last five years, mostly due to development of single molecule techniques, chiefly optical tweezers, allowing for manipulations and measurements of single kinesin molecules. Recently it has been established that neck linker plays a crucial role in kinesin motility, affects direction of movement and interacts with three loop regions in kinesin head core. It appeared that the key role of is mediated by specific interactions with the core which allow it to amplify subtle changes . Based on in-depth structural analysis and molecular dynamics simulation it has been recently proposed that, evolutionary conserved 9 to 13 -residue long N-terminal region, the cover strand, is essential in power-stroke like force generation and is plays crucial role in directionality. Upon the ATP binding switch II of leading head, with neck linker initially undocked, retracts allowing for the extra helical turn of $\alpha 6$ to coil initiating registering in frame of cover strand and $\beta 9$ so that they can form cover neck bundle leading to the power stroke. Once the forward movement is initiated the ASN latch and $\beta 10$ ensuring tight binding of neck linker to motor head. This plausible scenario is additionally supported by similar structural arrangements observed in other kinesin motors and thermodynamics analysis. Previously there has been only one mutagenesis study targeting neck linker region which showed that V331A/N332A mutation decreased the speed and stall force of kinesin. However there have never be a systematic mutagenesis study of neck linker/cover strand region which would be needed to test the

hypothesis and elucidate more details which might be useful in refining the mode.

We have designed such a study by engineering five kinesin mutants (1) a mutant in which cover strand is completely removed, which is expected to show no movement at all (2) Mutating two contact residues S12 and I13 to glycines to decrease interactions with the motor core, which is expected to adversely affect power stroke and hence the movement (3) Cleaving AA1-8 which is expected to remove a significant portion of neck linker showing effect similar to mutant (1) but allowing to define more finely the crucial region of cover strand (4) mutating A9G, E10G, D11G, S12G which should have similar effect as (2) but more severe and finally (5) mutating A9G and D11G, which is expected to affect the power stroke, but is the least severe of all mutations. Detailed experimentation was conducted only with the last mutant (5) using optical tweezers. Those experiments show that although step size for both the wild type kinesin and mutant kinesin is the same the mutant kinesin has lower stall force and slower both, loaded and unloaded, velocities. It also takes significantly more backwards steps and is more processive. Experimental results reinforce the proposed power stroke model showing that affected cover strand drastically affects the motion of the kinesin in a way that is consistent with cover neck initiated power stroke. When the formation of cover neck bundle is impaired the generated walking force is smaller and hence the lower stall forces, moreover the dwell times between the steps are longer while there are less interactions promoting cover neck bundle formation it takes longer, but when the step is initiated its size is the same as the native kinesin. This result also suggests a role of cover neck bundle rather than simply neck linker in directionality of movement.

However, in order to fully understand and test proposed movement mechanism further experimental investigation would be needed. We are currently conducting similar investigation on remaining mutants. Those further studies should shed some light on the mechanism of kinesin motility answering important questions about power stroke mechanism, directionality, processivity, velocity and stalling of kinesin motors which would add to the overall physical, mechanistic understanding of molecular motors.

Bibliography

- [1] Luby-Phelps K, Castle PE, Taylor DL, Lanni F, 1987 Hindered Diffusion of inter tracer particles in cytoplasm of mouse 3T3 cells. PNAS, 84:4910-13
- [2] Goldstein LS, Philp AV., The road less traveled: emerging principles of kinesin motor utilization, Annu Rev Cell Dev Biol. 1999;15:141-83.
- [3] Reid E, Kloos M, Ashley-Koch A, Hughes L, Bevan S, Svenson IK, Graham FL, Gaskell PC, Dearlove A, Pericak-Vance MA, Rubinsztein DC, Marchuk DA., A kinesin heavy chain (KIF5A) mutation in hereditary spastic paraplegia (SPG10), Am J Hum Genet. 2002 Nov;71(5):1189-94.
- [4] Bloom GS, Goldstein LS. Cruising along microtubule highways: how membranes move through the secretory pathway. J Cell Biol 1998;140:12771280.
- [5] Vale R.D, Fletterick R.J. The design plan of kinesin motors. Annu. Rev. Cell Dev. Biol. 13, 745-777 (1997).
- [6] Kull, F. J., Sablin, E. P., Lau, R., Fletterick, R. J. & Vale, R. D. Crystal structure of the kinesin motor domain reveals a structural similarity to myosin. Nature 380, 550-555 (1996).
- [7] Sablin, E. P., Kull, F. J., Cooke, R., Vale, R. D. & Fletterick, R. J. Crystal structure of the motor domain of the kinesin-related motor ncd. Nature 380, 555-559 (1996).
- [8] Case, R. B., Pierce, D. W., Hom-Booher, N., Hart, C. L. & Vale, R. D. The directional preference of kinesin motors is specified by an element outside of the motor catalytic domain. Cell 90, 959-966 (1997).

- [9] Henningsen, U. & Schliwa, M. Reversal in the direction of movement of a molecular motor. *Nature* 389, 93-96 (1997).
- [10] Endow, S. A. & Waligora, K. W. Determinants of kinesin motor polarity. *Science* 281, 1200-1202 (1998).
- [11] Howard, J., Hudspeth, A. J. & Vale, R. D. Movement of microtubules by single kinesin molecules. *Nature* 342, 154158 (1989).
- [12] Svoboda, K., Schmidt, C. F., Schnapp, B. J. & Block, S. M. Direct observation of kinesin stepping by optical trapping interferometry. *Nature* 365, 721727 (1993).
- [13] Vale, R. D., T. Funatsu, D. W. Pierce, L. Romberg, Y. Harada, and T. Yanagida. 1996. Direct observation of single kinesin molecules moving along microtubules. *Nature*. 380:451453.
- [14] Hancock, W. O. & Howard, J. Processivity of the motor protein kinesin requires two heads. *J. Cell Biol.* 140, 13951405 (1998).
- [15] Hackney, D. D. Evidence for alternating head catalysis by kinesin during microtubule-stimulated ATP hydrolysis. *Proc. Natl Acad. Sci. USA* 91, 68656869 (1994).
- [16] Ma, Y.-Z. & Taylor, E. W. Interacting head mechanism of microtubule-kinesin ATPase. *J. Biol. Chem.* 272, 724730 (1997).
- [17] Gilbert, S. P., Moyer, M. L. & Johnson, K. A. Alternating site mechanism of the kinesin ATPase. *Biochemistry* 37, 792799 (1998).
- [18] Arnal, I. & Wade, R. H. Nucleotide-dependent conformation of the kinesin dimer interacting with microtubules. *Structure* 1998, 3338 (1998).
- [19] Hirose, K., Lowe, J., Alonso, M., Cross, R. A. & Amos, L. A. Congruent docking of dimeric kinesin and ncd into three-dimensional electron cryomicroscopy maps of microtubule-motor ADP complexes. *Mol. Biol. Cell* 10, 20632074 (1999).
- [20] Hirose, K., Lockhart, A., Cross, R. A. & Amos, L. A. Three-dimensional cryoelectron microscopy of dimeric kinesin and ncd motor domains on microtubules. *Proc. Natl Acad. Sci. USA* 93, 95399544 (1996).
- [21] Romberg, L. & Vale, R. D. Chemomechanical cycle of kinesin differs from that of myosin. *Nature* 361, 168170 (1993).

- [22] Jiang,W. & Hackney,D. D. Monomeric kinesin head domains hydrolyze multiple ATP molecules before release from a microtubule. *J. Biol. Chem.* 272, 56165621 (1997).
- [23] Moyer,M. L., Gilbert,S. P. & Johnson,K. A. Pathway of ATP hydrolysis by monomeric and dimeric kinesin. *Biochemistry* 37, 800813 (1998).
- [24] Romberg,L., Pierce,D. W. & Vale,R. D. Role of the kinesin neck region in processive microtubule-based motility. *J. Cell. Biol.* 140, 14071416 (1998).
- [25] Visscher,K., Schnitzer,M. J. & Block,S. M. Single kinesin molecules studied with a molecular force clamp. *Nature* 400, 184189 (1999).
- [26] Coppin,C. M., Pierce,D. W., Hsu,L. & Vale,R. D. The load dependence of kinesin's mechanical cycle. *Proc. Natl Acad. Sci. USA* 94, 85398544 (1997).
- [27] Wade RH, Kozielski F, Structural links to kinesin directionality and movement, *Nature Structural Biology* 7, 456 - 460 (2000).
- [28] Kull, F.J., Sablin, E.P., Lau, R., Fletterick, R.J. & Vale, R.D. Crystal structure of the kinesin motor domain reveals a structural similarity to myosin. *Nature* 380, 555559 (1996).
- [29] Gulick, A.M., Song, H., Endow, S.A. & Rayment I. X-ray crystal structure of the yeast Kar3 motor domain complexed with Mg.ADP to 2.3 resolution. *Biochemistry* 37, 17691776 (1998).
- [30] Kozielski F, Sack S, Marx A, Thormahlen M, Schonbrunn E, Biou V, Thompson A, Mandelkow EM, Mandelkow E. . The crystal structure of dimeric kinesin and implications for microtubule-dependent motility. *Cell* 91, 985994 (1997).
- [31] Sablin EP, Case RB, Dai SC, Hart CL, Ruby A, Vale RD and Fletterick RJ (1998) Direction determination in the minus-end-directed kinesin motor ncd. *Nature*, 395, 813816.
- [32] Kozielski, F., De Bonis, S., Burmeister, W.P., Cohen-Addad, C. & Wade, R.H. The crystal structure of the minus-end-directed microtubule motor protein ncd reveals variable dimer conformations. *Struct. Fold. Des.* 7, 14071416 (1999).

- [33] Müller, J., Marx, A., Sack, S., Song, Y.-H. & Mandelkow, E. The structure of the nucleotide binding site of kinesin. *Biol. Chem.* 380, 981992 (1999).
- [34] Sack S, Muller J, Marx A, Thormahlen M, Mandelkow EM, Brady ST, Mandelkow E., X-ray structure of motor and neck domains from rat brain kinesin. *Biochemistry* 36, 1615516165 (1997).
- [35] Arnal, I., Metoz, F., DeBonis, S. & Wade, R.H. Three-dimensional structure of functional motor proteins on microtubules. *Curr. Biol.* 6, 12651270 (1996).
- [36] Hirose, K., Lockhart, A., Cross, R.A. & Amos, L.A. Three-dimensional cryoelectron microscopy of dimeric kinesin and ncd motor domains on microtubules. *PNAS, USA* 93, 95399544 (1996).
- [37] Sablin, E.P, Kull F.J, Cooke R, Vale R.D, Fletterick R.J, Crystal Structure of the motor domain of the kinesin-related motor ncd. *Nature* 380, 550-555 (1996).
- [38] Tripet, B., Vale, R.D. & Hodges, R.S. Demonstration of coiled-coil interactions within the kinesin neck region using synthetic peptides: implications for motor activity. *J. Biol. Chem.* 272, 89468956 (1997).
- [39] Gauger AK, Goldstein LSB, The *Drosophila* kinesin light chain. *J. Biol. Chem.*,1993, 268:13657-66.
- [40] Wade RH, Chrétien D. 1993. Cryoelectron microscopy of microtubules. 1993, *J. Struct. Biol.* 110:1-27
- [41] Howard J, Hudspeth AJ, Vale RD, Movement of microtubules by a single kinesin molecules, 1993, *Nature* 342:154-58
- [42] Huang T-G, Hackney DD. *Drosophila* kinesin minimal motor domain expressed in *Escherichia coli* *J. Biol. Chem.* 269:16493-501
- [43] Ray S, Meyhöfer E, Milligan RA, Howard J, Kinesin follows the microtubule's protofilament axis, 1993, *J. Cell Biol.* 121:1083-93
- [44] Harrison BC, Marchese-Ragona SP, Gilbert SP, Cheng N, Steven AC, Johnson KA. Kinesin decoration of the microtubule surface: one kinesin head per tubulin heterodimer. 1993, *Nature* 362:73-75
- [45] Hunt AJ, Gittes F, Howard J. The force exerted by a single kinesin molecule against a viscous load. 1993, *Biophys J.* 67:766-81

- [46] Gittes F, Meyhöfer E, Baek S, Howard J. Directional loading of the kinesin motor molecule as it buckles a microtubule 1996, *Biophys J* 70
- [47] Styer L. 1995, *Biochemistry*. 4th ed. New York, NY: W.H. Freeman & Co.
- [48] Block SM, Goldstein LSB, Schnapp BJ. Bead movement by a single kinesin molecules studied with optical tweezers. 1990, *Nature* 348:348-52
- [49] Berliner E., Young EC, Anderson K, Mahtani HK, Gelles J, Failure of single-headed kinesins to track parallel to protofilaments, 1995, *Nature* 373:718-21
- [50] Kawaguchi K, Ishiwata S., Nucleotide-dependent single- to double-headed binding of kinesin. *Science*. 2001 Jan 26;291(5504):667-9.
- [51] Kawaguchi K, Uemura S, Ishiwata S., Equilibrium and transition between single- and double-headed binding of kinesin as revealed by single-molecule mechanics., *Biophys J*. 2003 Feb;84(2 Pt 1):1103-13.
- [52] Asenjo AB, Krohn N, Sosa H., Configuration of the two kinesin motor domains during ATP hydrolysis., *Nat Struct Biol*. 2003 Oct;10(10):836-42
- [53] Hua W, Chung J, Gelles J., Distinguishing inchworm and hand-over-hand processive kinesin movement by neck rotation measurements, *Science*. 2002 Feb 1;295(5556):844-8.
- [54] Hua W, Young EC, Fleming ML, Gelles J, Coupling of kinesin steps to ATP hydrolysis., *Nature*. 1997 Jul 24;388(6640):390-3.
- [55] Hoenger A, Thormahlen M, Diaz-Avalos R, Doerhoefer M, Goldie KN, Muller J, Mandelkow E., A new look at the microtubule binding patterns of dimeric kinesins. *J Mol Biol*. 2000 Apr 14;297(5):1087-103.
- [56] Kikkawa M, Sablin EP, Okada Y, Yajima H, Fletterick RJ, Hirokawa N., Switch-based mechanism of kinesin motors., *Nature*. 2001 May 24;411(6836):439-45.
- [57] Ma, Y.-Z. & Taylor, E.W. Interacting head mechanism of microtubule-kinesin ATPase. *J. Biol. Chem*. 272, 724-730 (1997).

- [58] Sprang, S. R. G protein mechanism: insights from structural analysis. *Annu. Rev. Biochem.* 66, 639- 678 (1997).
- [59] Scheffzek, K. et al. The Ras-RasGAP complex: structural basis for GTPase activation and its loss in oncogenic Ras mutants. *Science* 277, 333-338 (1997).
- [60] Kjeldgaard, M., Nyborg, J. & Clark, B. F. The GTP binding motif: variations on a theme. *FASEB J.* 10, 1347-1368 (1996).
- [61] Song, H. & Endow, S. A. Decoupling of nucleotide- and microtubule-binding sites in a kinesin mutant. *Nature* 396, 587-590 (1998).
- [62] Asbury C, Fehr A, Block S, Kinesin moves by an asymmetric hand-over-hand mechanism. *Science*. 2003 Dec 19;302(5653):2130-4.
- [63] K. Visscher, M. J. Schnitzer, S. M. Block, Single kinesin molecules studied with a molecular force clamp., *Nature* 400,184 (1999).
- [64] A. Hoenger A, Thormahlen M, Diaz-Avalos R, Doerhoefer M, Goldie KN, Muller J, Mandelkow E., A new look at the microtubule binding patterns of dimeric kinesins. , *J. Mol. Biol.* 297, 1087 (2000).
- [65] Case RB, Rice S, Hart CL, Ly B, Vale RD, Role of the kinesin neck linker and catalytic core in microtubule-based motility. *Curr Biol.* 2000 Feb 10;10(3):157-60.
- [66] R.B. Case, D.W. Pierce, N. Hom-Booher, C.L. Hart and R.D. Vale, The directional preference of kinesin motors is specified by an element outside of the motor catalytic domain. *Cell* 90 (1997), pp. 959966.
- [67] U. Henningsen and M. Schliwa, Reversal in the direction of movement of a molecular motor. *Nature* 389 (1997), pp. 9396
- [68] L. Romberg, D.W. Pierce and R.D. Vale, Role of the kinesin neck region in processive microtubule-based motility. *J Cell Biol* 140 (1998), pp. 14071416.
- [69] M. Grummt, G. Woehlke, U. Henningsen, S. Fuchs, M. Schleicher and M. Schliwa, Importance of a flexible hinge near the motor domain in kinesin-driven motility. *EMBO J* 17 (1998), pp. 55365542.
- [70] E. C. Young, H. K. Mahtani, J. Gelles, One-headed kinesin derivatives move by a nonprocessive, low-duty ratio mechanism unlike that of two-headed kinesin., *Biochemistry* 37, 3467 (1998)

- [71] Y. Okada, N. Hirokawa, A processive single-headed motor: kinesin superfamily protein KIF1A., *Science* 283, 1152 (1999).
- [72] Y. Okada, N. Hirokawa, Mechanism of the single-headed processivity: diffusional anchoring between the K-loop of kinesin and the C terminus of tubulin., *PNAS. U.S.A.* 97, 640 (2000).
- [73] E. Berliner, E. C. Young, K. Anderson, H. K. Mahtani, J. Gelles, Failure of a single-headed kinesin to track parallel to microtubule protofilaments. *Nature* 373, 718 (1995).
- [74] J. Howard, The mechanics of force generation by kinesin. *Biophys J.* 1995 Apr;68(4 Suppl):245S-253S; 253S-255S. Review.
- [75] J. Howard, The Movement of Kinesin Along Microtubules, *Annual Reviews Physiol*, 1996, 58:703-29
- [76] Naber N., Cooke R, Pate E, Binding of ncd to microtubules induces a conformational change near the junction of the motor domain with the neck. *Biochemistry*, 36, 9681-9689
- [77] Rice S, Lin AW, Safer D, Hart CL, Naber N, Carragher BO, Cain SM, Pechatnikova E, Wilson-Kubalek EM, Whittaker M, Pate E, Cooke R, Taylor EW, Milligan RA, Vale RD. A structural change in the kinesin motor protein that drives motility. *Nature*. 1999 Dec 16;402(6763):778-84.
- [78] Skiniotis G, Surrey T, Altmann S, Gross H, Song YH, Mandelkow E, Hoenger A, Nucleotide-induced conformations in the neck region of dimeric kinesin, *EMBO J.* 2003 Apr 1;22(7):1518-28.
- [79] C. Asbury, A. Fehr, S. Block, Kinesin Moves by an Asymmetric Hand-Over-Hand Mechanism, *Science*. 2003 Dec 19;302(5653):2130-4
- [80] S. Block, C. Asbury, J. Shaevitz, M Lang, Probing the kinesin reaction cycle with a 2D optical force clamp, *Proc Natl Acad Sci U S A.* 2003 Mar 4;100(5):2351-6.
- [81] A. Yildiz, M. Tomishige, R. Vale, P. Selvin, Kinesin Walks Hand-Over-Hand, *Science*. 2004 Jan 30;303(5658):676-8.
- [82] Higuchi H, Bronner CE, Park HW, Endow SA. Rapid double 8-nm steps by a kinesin mutant, *EMBO J.* 2004 Aug 4;23(15):2993-9.

- [83] Hirose K, Akimaru E, Akiba T, Endow SA, Amos LA, Large conformational changes in a kinesin motor catalyzed by interaction with microtubules. *Mol Cell*. 2006 Sep 15;23(6):913-23.
- [84] Tomishige M, Stuurman N, Vale RD., Single-molecule observations of neck linker conformational changes in the kinesin motor protein. *Nat Struct Mol Biol*. 2006 Oct;13(10):887-94.
- [85] Jaud J, Bathe F, Schliwa M, Rief M, Woehlke G., Flexibility of the neck domain enhances Kinesin-1 motility under load. *Biophys J*. 2006 Aug 15;91(4):1407-12.
- [86] L.A. Amos, Kinesin sticks its neck out. *Nat Cell Biol*. 2000 Jan;2(1):E15-6.
- [87] W. Hwang, M.J. Lang, M. Karplus, Force Generation in Kinesin hinges on cover-neck bundle formation
- [88] Ashkin, A. (1969) Acceleration and trapping of particles by radiation pressure. *Phys. Rev. Lett.* 24, 156159
- [89] Ashkin, A. and Dziedzic, J.M. (1987) Optical trapping and manipulation of viruses and bacteria. *Science* 235, 15171520.
- [90] Huber, R., Burggraf, S., Mayer, T., Barns, S.M., Rossnagel, P. and Stetter, K.O. (1995) Isolation of a hyperthermophilic archaeum predicted by in situ RNA analysis. *Nature* 376, 5758.
- [91] Vale RD, Milligan RA., The way things move: looking under the hood of molecular motor proteins. *Science*. 2000 Apr 7;288(5463):88-95.
- [92] Svoboda, K., Schmidt, C.F., Branton, D. and Block, S.M. (1992) Conformation and elasticity of the isolated red blood cell membrane skeleton. *Biophys. J.* 63, 784793
- [93] Seeger, S., Monajembashi, S., Hutter, K.J., Futterman, G., Wolfrum, J. and Greulich, K.O. (1991) Application of laser optical tweezers in immunology and molecular genetics. *Cytometry*. 12, 497504
- [94] Smith, S.B., Finzi, L. and Bustamante, C. (1992) Direct mechanical measurements of the elasticity of single DNA molecules by using magnetic beads. *Science* 258, 11221126

- [95] Smith, S.B., Cui, Y. and Bustamante, C. (1996) Overstretching B-DNA: the elastic response of individual double-stranded and single-stranded DNA molecules. *Science* 271, 795799
- [96] Williams, M.C., Wenner, J.R., Rouzina, I. and Bloomfield, V.A. (2001a) Effect of pH on the overstretching transition of double-stranded DNA: evidence of force-induced DNA melting. *Biophys. J.* 80, 874881
- [97] Bockelmann, U. (2004) Single-molecule manipulation of nucleic acids. *Curr. Opin. Struct. Biol.* 14, 368373
- [98] Stone, M.D., Bryant, Z., Crisona, N.J., Smith, S.B., Vologodskii, A., Bustamante, C. and Cozzarelli, N.R. (2003) Chirality sensing by *Escherichia coli* topoisomerase IV and the mechanism of typeII topoisomerases. *Proc. Natl. Acad. Sci. U.S.A.* 100, 86548659
- [99] Dumont, S., Cheng, W., Serebrov, V., Beran, R.K., Tinoco, Jr, I., Pyle, A.M. and Bustamante, C. (2006) RNA translocation and unwinding mechanism of HCV NS3 helicase and its coordination by ATP. *Nature* 439, 105108
- [100] Perkins, T.T., Dalal, R.V., Mitsis, P.G. and Block, S.M. (2003) Sequence-dependent pausing of single lambda exonuclease molecules. *Science* 301, 19141918
- [101] Pease, P.J., Levy, O., Cost, G.J., Gore, J., Ptacin, J.L., Sherratt, D., Bustamante, C. and Cozzarelli, N.R. (2005) Sequence-directed DNA translocation by purified FtsK. *Science* 307, 586590
- [102] Chemla, Y.R., Aathavan, K., Michaelis, J., Grimes, S., Jardine, P.J., Anderson, D.L. and Bustamante, C. (2005) Mechanism of force generation of a viral DNA packaging motor. *Cell* 122, 683692
- [103] Felgner, H., Frank, R. and Schliwa, M. (1996) Flexural rigidity of microtubules measured with the use of optical tweezers. *J. Cell Sci.* 109 (Pt 2), 509516
- [104] Tsuda, Y., Yasutake, H., Ishijima, A. and Yanagida, T. (1996) Torsional rigidity of single actin filaments and actin-actin bond breaking force under torsion measured directly by in vitro micromanipulation. *Proc. Natl. Acad. Sci. U.S.A.* 93, 1293712942

- [105] Tskhovrebova, L., Trinick, J., Sleep, J.A. and Simmons, R.M. (1997) Elasticity and unfolding of single molecules of the giant muscle protein titin. *Nature* 387, 308312
- [106] Cecconi, C., Shank, E.A., Bustamante, C. and Marqusee, S. (2005) Direct observation of the three-state folding of a single protein molecule. *Science* 309, 20572060
- [107] Wang, Z., Khan, S. and Sheetz, M.P. (1995) Single cytoplasmic dynein molecule movements: characterization and comparison with kinesin. *Biophys. J.* 69, 20112023
- [108] Iner, J.T., Simmons, R.M. and Spudich, J.A. (1994) Single myosin molecule mechanics: piconewton forces and nanometre steps. *Nature* 368, 113119
- [109] Mehta, A.D., Rock, R.S., Rief, M., Spudich, J.A., Mooseker, M.S. and Cheney, R.E. (1999) Myosin-V is a processive actin-based motor. *Nature* 400, 590593
- [110] Rock, R.S., Rice, S.E., Wells, A.L., Purcell, T.J., Spudich, J.A. and Sweeney, H.L. (2001) Myosin VI is a processive motor with a large step size. *Proc. Natl. Acad. Sci. U.S.A.* 98, 1365513659
- [111] Ghislain, L.P. and Webb, W.W. (1993) Scanning-force microscope based on an optical trap. *Opt. Lett.* 18, 16781680
- [112] Florin, E.L., Pralle, A., Horber, J.K. and Stelzer, E.H. (1997) Photonic force microscope based on optical tweezers and two-photon excitation for biological applications. *J. Struct. Biol.* 119, 202211
- [113] Nobel Prize in Physics in 1997 to S. Chu, C. Cohen-Tannoudji and W.D. Phillips, Nobel Lecture
- [114] Ketterle, W. (1999) Experimental studies of BoseEinstein condensation. *Phys. Today* 52, 3035
- [115] Balykin, V.I. and Letokhov, V.S. (1989) Laser optics of neutral atomic beams. *Phys. Today* 42, 2328
- [116] Kasevich, M. and Chu, S. (1991) Atomic interferometry using stimulated raman transitions. *Phys. Rev. Lett.* 67, 181184
- [117] Schnitzer, M. J, Block, S. M. (1997) *Nature* 388, 386-390

- [118] E. Hecht, *Optics*, Addison Wesley, 2001
- [119] Kaseda K, Higuchi H, Hirose K. Alternate fast and slow stepping of a heterodimeric kinesin molecule. *Nat Cell Biol.* 2003 Dec;5(12):1079-82.
- [120] Svoboda K, Block SM., Force and velocity measured for single kinesin molecules. *Cell.* 1994 Jun 3;77(5):773-84.
- [121] Kikkawa M, Okada Y, Hirokawa N, 15 A resolution model of the monomeric kinesin motor, KIF1A., *Cell.* 2000 Jan 21;100(2):241-52.
- [122] Sablin EP, Fletterick RJ., Abstract Nucleotide switches in molecular motors: structural analysis of kinesins and myosins. *Curr Opin Struct Biol.* 2001 Dec;11(6):716-24.
- [123] Kull FJ, Endow SA., Kinesin: switch I & II and the motor mechanism., *J Cell Sci.* 2002 Jan 1;115(Pt 1):15-23.
- [124] Sindelar CV, Budny MJ, Rice S, Naber N, Fletterick R, Cooke R.
- [125] Oster G, Wang H, How Protein Motors Convert Chemical Energy into Mechanical Work Chapter 8 of *Molecular Motors*. Wiley, 2003
- [126] Mather, W. H. and Fox, R. F. (2006). Kinesins biased stepping mechanism: Amplification of neck linker zippering. *Biophys. J.* 91, 24162426.
- [127] Neuman KC, Block SM., Optical trapping., *Rev Sci Instrum.* 2004 Sep;75(9):2787-2809.
- [128] Chu S, Bjorkholm JE, Ashkin A, Cable A., Experimental observation of optically trapped atoms., *Phys Rev Lett.* 1986 Jul 21;57(3):314-317.
- [129] Brau RR, Tarsa PB, Ferrer JM, Lee P, Lang MJ, Interlaced optical force-fluorescence measurements for single molecule biophysics. *Biophys J.* 2006 Aug 1;91(3):1069-77.
- [130] Wade RH, Kozielski F., Structural links to kinesin directionality and movement. *Nat Struct Biol.* 2000 Jun;7(6):456-60.
- [131] Hwan W, Lang M., Karplus M, Force Generation in kinesin hinges on cover-neck bundle formation, 2007, manuscript in preparation
- [132] Tomishige M, Vale RD. , Controlling kinesin by reversible disulfide cross-linking. Identifying the motility-producing conformational change. *J Cell Biol.* 2000 Nov 27;151(5):1081-92.

- [133] Addas KM, Schmidt CF, Tang JX., Microrheology of solutions of semi-flexible biopolymer filaments using laser tweezers interferometry. *Phys Rev E Stat Nonlin Soft Matter Phys.* 2004 Aug;70(2 Pt 1):021503.
- [134] Appleyard D.C., Vandermeulen K.Y., Lang M. J, Optical Trapping for Undergraduates (manuscript)
- [135] Crocker, John C. and Grier, David G., When Like Charges Attract: The Effects of Geometrical Confinement on Long-Range Colloidal Interactions, *Phys. Rev. Lett.* 77 (9), pp. 1897–1900, (Aug 1996).
- [136] Carter NJ, Cross RA, Mechanics of the kinesin step, *Nature.* 2005 May 19;435(7040):308-12.
- [137] A. Savitzky and Marcel J.E. Golay (1964). Smoothing and Differentiation of Data by Simplified Least Squares Procedures. *Analytical Chemistry*, 36: 1627-1639.
- [138] P.L. Rosin, "Unimodal thresholding", *Pattern Recognition*, vol. 34, no. 11, pp. 2083-2096, 2001.
- [139] Abbondanzieri EA, Greenleaf WJ, Shaevitz JW, Landick R, Block SM, Direct observation of base-pair stepping by RNA polymerase. *Nature.* 2005 Nov 24;438(7067):460-5. Epub 2005 Nov 13.
- [140] Visscher K, Schnitzer MJ, Block SM., Single kinesin molecules studied with a molecular force clamp. *Nature.* 1999 Jul 8;400(6740):184-9.
- [141] Nishiyama M, Muto E, Inoue Y, Yanagida T, Higuchi H., Substeps within the 8-nm step of the ATPase cycle of single kinesin molecules., *Nat Cell Biol.* 2001 Apr;3(4):425-8. [Click here to read](#)
- [142] Rosenfeld SS, Jefferson GM, King PH., ATP reorients the neck linker of kinesin in two sequential steps., *J Biol Chem.* 2001 Oct 26;276(43):40167-74
- [143] Hormeno S, Arias-Gonzales R., Exploring mechanochemical processes in the cell with optical tweezers, *Cell* (2006), 679-695
- [144] Nicholas R. Guydosh, Steven M. Block, Backsteps induced by nucleotide analogs suggest the front head of kinesin is gated by strain, *PNAS* 2006, 80548059, vol. 103 (21)